# ABSTRACT


Title of thesis: A STUDY OF INTERMITTENT CONVECTIVE HEATING EFFECTS ON FINE FUEL IGNITION

Lana Benny, Master of Science, 2019

Thesis directed by: Professor Michael J. Gollner
Department of Fire Protection Engineering

Recent studies have suggested the potential importance of intermittent convective heating on the ignition of fine fuels during wildland fire spread. In this study, a novel pulsed-gas line burner similar to a Rubens' tube, driven by acoustic oscillations, is used to re-create the pulsations observed in wildland fires in a controlled environment. After acoustically stimulating a long tube with perforations at the top, creating a pulsed linear flame, thin fuels with different densities and diameters are quickly placed in the center of the flame. The temperature of these fuels is measured using an infrared camera, distinguishing the temperature at which the fuel starts to pyrolyze. As expected, smaller-diameter fuels ignite faster when exposed to flames; however, they also are least affected by intermittent heating. Larger-diameter fuels are more dramatically affected by intermittent heating frequencies, in large part due to cooling effects between pulses and the larger thermal mass of the fuels. The results are discussed and compared with a simple numerical model incorporating measured velocities and temperatures present in the burner and their effect on a thermally-thin fuel element over time.

# A STUDY OF INTERMITTENT CONVECTIVE HEATING EFFECTS ON FINE FUEL IGNITION

by

Lana Benny

Thesis submitted to the Faculty of the Graduate School of the
University of Maryland, College Park in partial fulfillment
of the requirements for the degree of
Master of Science
2019

Advisory Committee:

Associate Professor Michael J. Gollner, Chair
Professor James A. Milke
Dr. Sara McAllister

# Acknowledgments

I would like to express my sincere gratitude to my supervisor, Dr. Michael J. Gollner, for his continuous encouragement and advice which has significantly helped me succeed in the completion of my dissertation.

I would like to thank Dr. James Milke, for sharing his expertise, and valuable guidance and encouragement towards this project.

I extend my appreciation to all the faculty members for their assistance. I thank my parents for their unceasing encouragement, support and attention.

I am tremendously grateful to my friends in the department for their assistance in the project. Nicholas Warner and Nicholas Chui for helping me run a lot of tests to gather data and help bring this project to fruition.

Lastly, I would like to thank Matthew Weston-Dawkes, Ajay Singh, Conor McCoy and Evan Sluder for their efforts aiding in the development and initial use of this apparatus. This research was funded by the National Science Foundation under Grant No. CBET-1554026.

# Table of Contents

# List of Figures

# List of Tables

# Nomenclature

| | |
|---|---|
| $c_p$ | Specific heat at constant pressure (J/kg-K) |
| $D$ | Species diffusivity ($m^2/s$) |
| $d$ | Diameter (m) |
| $g$ | Gravitational acceleration ($m/s^2$) |
| Gr | Grashof number (-) |
| $h$ | Convective heat transfer coefficient ($W/m^2$-K) |
| $h_g, \Delta H_g$ | Effective heat of gasification or vaporization (J/kg) |
| $\Delta H_c$ | Heat of combustion per unit mass of oxygen (J/kg) |
| $k$ | Thermal conductivity (W/m-K) |
| $L$ | Length of the fuel surface (m) |
| $\dot{m}_f{}''$ | Mass-burning rate (mass flux) ($kg/m^2$-s) |
| Nu | Nusselt number (-) |
| Pr | Prandtl number (-) |
| $\dot{q}''_{net}$ | Net heat flux ($W/m^2$) |
| $\dot{q}''_{fl,c}$ | Convective heat flux ($W/m^2$) |
| $\dot{q}''_{fl,r}$ | Radiative heat flux ($W/m^2$) |
| $\dot{q}''_{s,rr}$ | Surface Re-radiation heat flux ($W/m^2$) |
| $\dot{q}''_{s,i}$ | Incident heat flux ($W/m^2$) |
| Re | Reynolds number (-) |
| Ri | Richardson number (-) |
| $t$ | Time (s) |
| $T$ | Temperature (K) |
| $T^*$ | Non-dimensional temperature (-) |
| $y_f$ | Flame standoff distance (m) |

# Nomenclature

**Greek Symbols**

| | |
|---|---|
| $\alpha$ | Thermal diffusivity ($m^2/s$) |
| $\varepsilon$ | Emissivity (-) |
| $\nu$ | Kinematic viscosity ($m^2/s$) |
| $\rho$ | Density ($kg/m^3$) |

**Subscripts**

| | |
|---|---|
| $ad$ | Adiabatic |
| $f$ | Film (mean properties) |
| $fl$ | Flame |
| $g$ | Gas |
| $\infty$ | Ambient |
| $p$ | Pyrolysis |
| $s$ | Surface |
| $ig$ | Ignition |
| $tc, b$ | Thermocouple junction or bead |
| $w$ | Wall |

**Abbreviations**

| | |
|---|---|
| WUI | Wildland Urban Interface |
| FBAN | Fire Behavior Analysts |
| SAVR | Surface Area to Volume Ratio |
| WFDS | Wildland-Urban Interface Fire Dynamics Simulator |
| CFD | Computational Fluid Dynamics |
| NIST | The National Institute of Standards and Technology |
| FDS | Fire Dynamics Simulator |

# Chapter 1

# Problem Statement

## 1.1 Introduction

Over the past decade, the number of fires in the U.S. have decreased but the size and severity of these fires have increased drastically [1]. These large wildland fires pose a growing threat to local populations and natural resources [2, 3]. A critical need for the management and mitigation of these fires is to accurately model their spread. Current models, however, are not physically based and it is desired to create a model to predict the propagation of wildland fires based on heat transfer, fluid dynamics and combustion processes [4]. While changes in wind or slope strongly affect the rate of spread of a wildland fire, the effect of convective heating contributing to ignition of vegetation and ultimately flame spread is largely unknown [5]. Convective heating of thin fuel elements such as pine needles, grass, etc. appears to be a critical but under-studied element of fire spread that could help the current models better describe the physics of wildland fires [4, 6].

New observations have revealed that a significant driver of heating in wind-driven fires come as periodic, forward pulsations of flames and hot gases that contact thin

vegetative fuel elements intermittently [6]. Existing, radiation-driven spread models need to incorporate this intermittent direct flame contact, however the source and structure of these pulsations or bursts have not been clearly identified or modeled [5]. Several observed structures, such as stream-wise streaks and span-wise waves similar to fluid flow phenomena appear to generate these pulsations, but the mechanism for their formation or predictive tools to model their effects do not exist. The frequency of these pulsations, however, have been measured, in the range of 0.5 to 10 Hz, but their direct effect on ignition and fire spread has not been established [6]. To develop a more accurate fire spread model, research must be performed to understand the nature of this intermittent flame contact and the factors that influence it's effect on the ignition of fine fuels, which typically drive wildland fire spread.

### 1.1.1 Wildfire trends

Wildfires in the United States have been increasing in size, duration and frequency since at least the mid 1980's [7]. Fire exclusion, climate change, and the movement of populations into the Wildland-Urban Interface (WUI) areas have influenced the frequency and severity of wildfires. Climate change has been cited as a particularly strong driver worsening the trends. As global temperatures increase, moisture and precipitation levels change, generally making wet areas wetter and dry areas drier [8]. Higher temperatures in the summer and spring combined with early spring snow melt cause soils to become drier than normal. This increases the likelihood of drought and might lead to a longer, more severe fire season. In addition, resultant changes

in vegetation patterns and fire regimes play an important role. These conditions create wildfires that are more intense and burn larger areas for longer times. Other factors such as fuel availability and human activity play a role in fire activity. Current predictions show that temperatures and precipitation are projected to change over the course of the century, with the potential for wildfire severity increase in many areas [9].

## 1.2 Need for an Improved Model of Wildland Fire Spread

Wildfires are destructive and often occur around WUI areas. These fires are hard to control and manage, often shifting directions due to changing environmental conditions. Historically, the desire to understand fire spread was motivated by the need for reliable predictions of where a fire will be in the future, mostly to plan suppression operations. With rapid technological advancements over the past several decades, single one-dimensional models have been adapted for use in two and three dimensional simulations of fire spread for applications ranging from real-time predictions to risk assessments [10]. The Rothermel model, a 1-D, energy balance based semi-empirical equation was a significant contribution to the field in terms of understanding and quantifying wildland fire spread [11]. The same model, however, is still used as the basis for state-of-the-art coupled fire-weather applications such as FARSITE.

For an effective response to wildland fires, the ability to model and predict the movement of fire is required. Equations and models are used to obtain predictions

and to understand wildland fire behavior. Current models used are empirical in nature [12] and linked to large scale observations of fire spread, fuel models, and moisture content levels, etc.

In addition to these empirical approaches, some more physically-based models have attempted to understand the physical processes responsible for the wildfire behavior by incorporating the applicable physics and chemistry [13]. However, even these models must make some assumptions about the fundamental processes of fire spread and ignition without any experimental basis. The lack of a common formulation for the physical and chemical processes in the physically-based models points out that a crucial theory in wildland fire spread is still missing.

## 1.3 Summary

The work presented in this thesis attempts to add to our knowledge of fire behavior by experimentally examining the influence of intermittent convective heating to fine wildland fuels. Following the results from the experiments, the role of intermittent heating is numerically simulated using a simple heat transfer based model of heating and cooling over fine fuels. Using this approach, it should be possible to estimate ignition times and, thus, fire spread. If the behavior of the flame front is already known, the need to create an improved model for wildfire spread will be discussed.

# Chapter 2

# Literature Review

The design of and interest in pulsating burners is not a recent phenomenon. Research on pulsating burners began at least twenty years ago. The goal of previous research has been for the design of more efficient combustion processes. Zinn et al. studied the physical mechanisms in pulsed combustors to make recommendations for a better design of a novel pulsed combustor [14]. Delabroy et al. later studied the effect of pulsations on the exhaust levels of nitric oxides [15]. Unlike previous work, this project uses a pulsating burner (Rubens' Tube) to study the ignition and heat transfer mechanisms impacting fine fuels during wildland fire spread. The application of this research is to obtain a better understanding of wildland fire ignition in which pulsations have been observed when convective cooling is taken into consideration. Ignition times across frequencies between 0-5 Hz and varying fuel diameter sizes are closely studied using different fine fuels.

## 2.1 Predicting fire behavior

In a wildland fire, neglecting fuels, the rate of fire spread is increased by a low fuel moisture content, wind, and sloped surfaces, and decelerated by increased fuel moisture and downward slopes. Rothermel's semi-empirical model was one of the most substantial contributions in the field of wildland fires. The equation, semi-empirically predicting the rate of fire spread, has been adopted at the core for most wildfire simulations in the United States [11]. Due to its empiricism, however, the formulation does not explain the modes of heat transfer contributing to flame spread, cannot model the start or stop of a fire, cannot incorporate acceleration or deceleration, and more importantly, is not necessarily valid beyond previously-tested limits. It is currently implemented in operational models such as BEHAVE [16] and FARSITE [17].

Recent work by Finney et al. helped to improve our current understanding of fire dynamics contributing to wildfire spread [6]. Their theory for fire spread relates observed fluid mechanics features in the flow and their effect on generating intermittent structures, to downstream heat transfer, using field and laboratory experiments to present their results. They propose that the method of heat transfer in fine fuels is dominated by intermittent flame contact, mainly driven by upstream convective flows. Because wildland fuels that carry fire are incredibly small in diameter, they are uniquely affected by direct flame contact as convective cooling limits the role of radiative heating. Conducting tests to better understand the role of flame intermittency on fine fuel ignition could therefore help to improve future

wildfire predictions.

Albini and Reinhardt presented a study on the ignition time of wooden dowels. In their work, they developed predictive equations for ignition time delay and burning rate for large woody fuels by deriving relationships between fuel properties and temperatures in a fire environment [18]. Lamorlette et al. theoretically investigated the impact of intermittent heating in a diffusion flame model [19]. Most other studies which have investigated intermittent heating have focused on lower frequency radiative heating changes to thermally-thick fuels, different than what occurs to thermally-thin fuels in wildland fires [20, 21, 22].

### 2.1.1 Rothermel's Model

Fire modeling is used to understand aspects of fire ecology, management, suppression and hazard assessment. One of the major components of modeling involves describing the environment (weather, fuel type and topography) and its effect on fire behavior, such as the fire intensity, rate of spread, etc. Rothermel's surface fire spread model is the most well-used model in U.S. fire management system.

The model, categorized as a semi-empirical model, is based on the work of Frandsen [23], data from wind tunnel experiments and data from field experiments [24]. Initially it was used to quantitatively calculate U.S. fire danger rating indices [25] and later as a tool for predicting the behavior of an ongoing fire [26]. The model is now incorporated into many wildfire prediction software packages for example, BehavePlus [16] and

FARSITE [17].

The model is based on a conservation of energy, best described by a heat source divided by a heat sink [23]. Assuming a linear flame front, it calculates the flame spread rate of a head fire with or without wind and or slope. The schematic of the different fire behaviors are represented in figure 2.1.1.

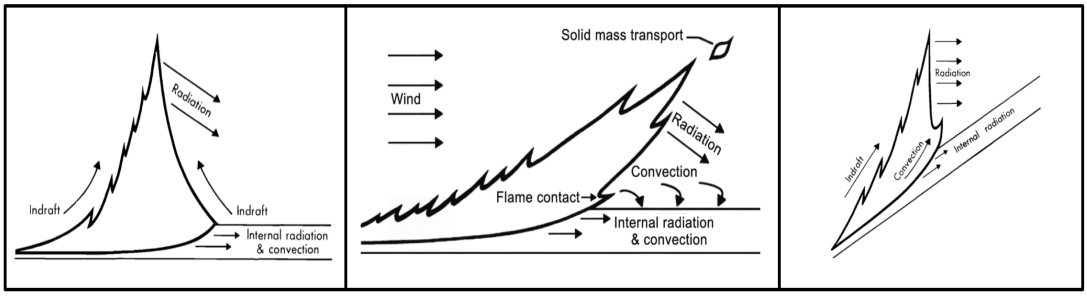


Figure 2.1.1: Schematic of (a) no wind fire, (b) wind-driven fire, (c) up-slope fire [26, 27, 28]

This model is valid for a fire going upwards on a slope with or without the presence of wind over a uniform fuel-bed. Fuels can consist of a mixture of various size classes of live and dead fuel represented over a single layer of depth. The most influential fuel component in this model is fine dead fuel. It can address fire for surface fuel up to a height of 6 ft tall which tends to include brush and small trees. Rothermel's model is not applicable to a crown fire in over-story trees, ground-based smoldering fire and combustion of fuels that burn after the flame front has passed as it was designed to use fuel, moisture and terrain data prior to ignition. It has associated modules to calculate flame length, spread direction, fuel moisture, etc. making it applicable over a range of applications. However, the model makes some strong assumptions like a

steady rate of spread and uniform, dead fuel bed properties which do not represent realistic inhomogenous wildland fuels. This limits the results from being completely accurate in real-world scenarios showing that there is a need to build a better, more holistic model. The equation's strength lies in the simplicity of input requirements, calculations and the freedom to change many of the driving variables. Being able to change the fuel parameters, a feature not available within statistical models developed for specific fuel and fire behavior types, makes this an extremely customizable and useful wildfire model.

The basic Rothermel model with minor modifications by Albini [18] has been in use for decades.

## 2.2 Fuel type and classification

Wildland fuels are made of various components of vegetation, both live and dead in a chosen area. The quality and type depends on the climate, soil, geography and fire history of the location. To a large extent, studies of annual precipitation, altitude and topography have been used for vegetation maps [29]. An adequate description of fuel often requires identifying the fuel components that may exist. This includes litter and duff layers, woody material, grasses, shrubs, timber and slash, to name a few. Significant features within each fuel component contribute to the selection of an appropriate fuel model from Scott et al. [30] to estimate fire behavior. Fuel loading, size class, distribution of load and its arrangement govern whether an ignition will result in a sustaining fire. Horizontal continuity influences whether a fire will spread

or not and how steady the rate of spread will be. Low fuel moisture content has a significant impact upon fire behavior affecting ignition, spread and intensity.

The original 13 fire behavior fuel models suggested by Anderson [27] have worked well to predict spread rate and intensity. The creation of a 40 model fire behavior have been able to cover a larger range of circumstances namely, prescribed fire, wildland fire use, simulating transition from a crown fire using crown fire initiation models.

It is known that smaller fuels ignite more readily than larger ones. The rapidity with which small fuels can be heated and ignited makes it an important factor to determine fire spread in surface fires. The time required to heat a fine fuel to ignition greatly depends on its Surface Area to Volume Ratio (SAVR). This ratio increases rapidly as the fuel size decreases. Small-sized fuels burn more rapidly than larger fuels and heat is released within a shorter period of time with a lower moisture content and greater SAVR. Dead and woody fuels have been grouped into classes that reflect the rate at which they can respond to change in atmospheric conditions, generally classified as seen in Table 2.1. Small fuels have also been found to increase the chances of ignition within a fuel bed, such as via small firebrands [31].

Fuel models describe the amount and physical characteristics of live and dead fuel. Dead fuel size classes are based on how rapidly a given fuel particle responds to environmental changes. The time lag (time for a dead fuel particle to lose 63% of its initial moisture content by mass) is used to group fuels into size classes by diameter (1-hr, 10-hr, 100-hr). Live fuel classes are further characterized as woody or herbaceous. The moisture dynamics between a live and dead fuel differ since live fuels are driven by the development stages of a plant and don't readily release moisture

as does a dead fuel. Studies have shown that fire models are extremely sensitive to changes in live fuel moisture and highlight that small changes in the live fuel moisture content cause large changes in the predicted fire behavior [32].

Table 2.1: Frequency Selection

| **Timelag** | **Diameter (cm)** |
|---|---|
| 1 - hr | $< 0.6$ |
| 10 - hr | 0.6 - 2.5 |
| 100 - hr | 2.5 - 7.6 |
| 1000 - hr | 7.6 - 20.3 |

The fuel moisture content of extinction is the moisture above which fuels will no longer burn. It is calculated as a function of three variables: dead fuel moisture, dead fuel moisture of extinction and ratio of live to total fuel. This makes the new 40 fuel models by Scott and Burgen more complicated due to its dynamic nature. It not only varies the live fuel moisture but also the ratio of live fuel loading to dead fuel loading.


Figure 2.2.1: Types of fine fuel

Small 1 - hr fuels generally consist of dry grass, pine needles, twings and leaves [Figure 2.2.1]. These fuels are also called flashy fuels due to their rapid ignition and burning behavior. Even though fine fuels exchange moisture rapidly, they release off moisture

very slowly when on the ground. The moisture in pine needles, for instance, stay moist due to sunlight and air only being exposed to the top layer, making it act more like a larger fuel.

## 2.3 Role of intermittent heating and cooling

Since ignition is the foundation of wildfire spread [33], understanding fuel particle heat exchange, ignition processes, and the conditions for sustained ignition is required as a basis for predicting fire spread and its resultant spread rate. Before looking into ignition, the flame front must be studied. Flames often consist of three regions: a continuous flame, an intermittent region where flames fluctuate in appearance, and a buoyant plume of heated gases following the flame [34].

These regions are not dissimilar from observations in wildland fire, however flames often lay down closer to the fuel surface when acted upon by wind or slope. It is in the middle, intermittent region where recent studies by Finney et al. [6] have focused.

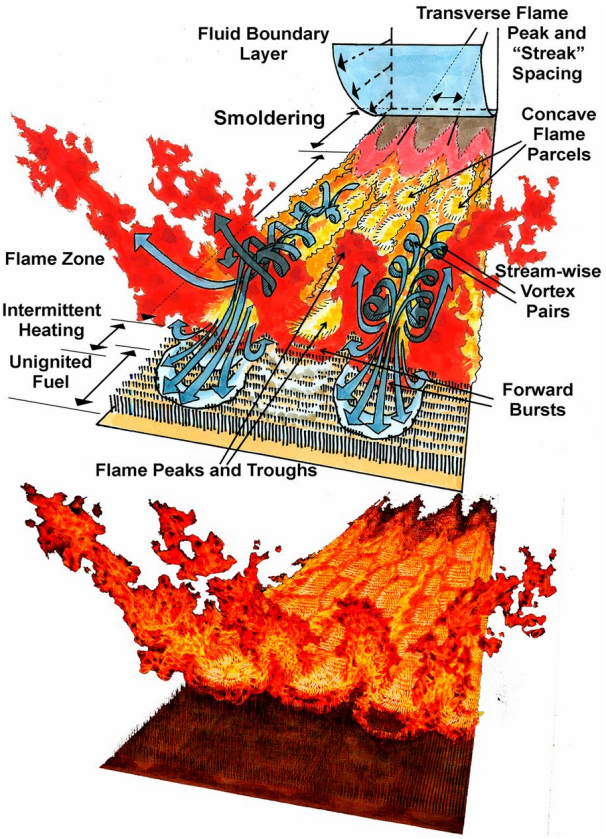


Figure 2.3.1: The different flame regions observed in a spreading wildland fire flame front by Finney et al. [6]

Research has yet to reveal how convection or flame contact plays a role in fuel ignition in wildland fires. The intermittent heating and cooling in this case refers to the heating of the fuel by flame impingement [35]. Byram et al. in their work on wooden cribs observed the flame contacts ahead of the burning zone playing a role in fire spread and ignition [36]. Similar observations were made by Rothermel and Anderson [37] and Albini [38]. Experiments conducted by Vogel and Williams [39] and Carrier et al. [40] stated that the role of flame contact determined the spread rate of the flame. With the notion of intermittent flame contact, Clark et al. [41] and Coen et al. [42] reported forward-pulsing flames as the primary cause for the spread of

large crown fires. Despite these observations, radiation is still generally used as the dominant heat transfer mechanism in wildland fire models.

Including convective fuel heating into fire spread models requires some assumptions along with the presence of unknown parameters. Understanding the characteristics of this heating and cooling via convection would greatly improve the reliability of future wildfire models and help predict fire spread.

## 2.4 Effects of radiation and convection

From the start of fire research, radiation has been assumed as the principal heating mechanism responsible for wildfire spread [43]. Sen and Puri in their work have identified radiation as the main heat transfer mechanism for different combustion processes [44]. While radiation has been identified as the important factor in fire spread and ignition, analysis of other heat transfer mechanisms such as convection have yet to be studied. Baines in his work mentioned processes like: convective cooling to the atmosphere, radiation from the heated part of the fuel bed and conduction downward and through the fuel-bed may cool the fuel-bed and influence the heat content [45]. de Mestre et al. presented a theoretical model assuming a steady-state configuration relative to the fire front, where the fuel bed is assumed to be heated by radiation from the flame and the fuel bed cooled by radiation from the fuel bed to space and by convective cooling [46]. Convective cooling was assumed to follow a Newtonian law with a constant convection coefficient to the model of de Mestre et al. Incropera and de Witt gave a methodology for calculating values of $h$ for heated

objects of various shapes, based on Nusselt number, when the cooling is due to either natural convection or an externally imposed flow [47].

Work on wildfire modeling by Albini played a significant role in establishing radiation as the governing mechanism of fire spread [18]. The assumption of radiation playing a key role in fire spread without an experimental basis has become a standard premise for other modelers. He assumed the flame front to be a steady radiating planar surface in both surface and crown fire spread model. Although Albini recognized convective cooling of pre-heated fuels from fire-induced inflow, it was not taken further.

The assumption of radiation as a singular factor has not be accepted easily. Baines [45] and Weber [48] mentioned that the preheating of fuel particles ahead of the flame zone was not accounted for in radiation-driven models. The temperature of fuel during preheating (measured by de Mestre et al. [46]) had a different profile than that predicted by radiation models. The addition of convective cooling resulted in profiles that were close to the experimental measurement until the flame front to fuel distances were withing a few centimeters, shown in Figure 2.4.1.

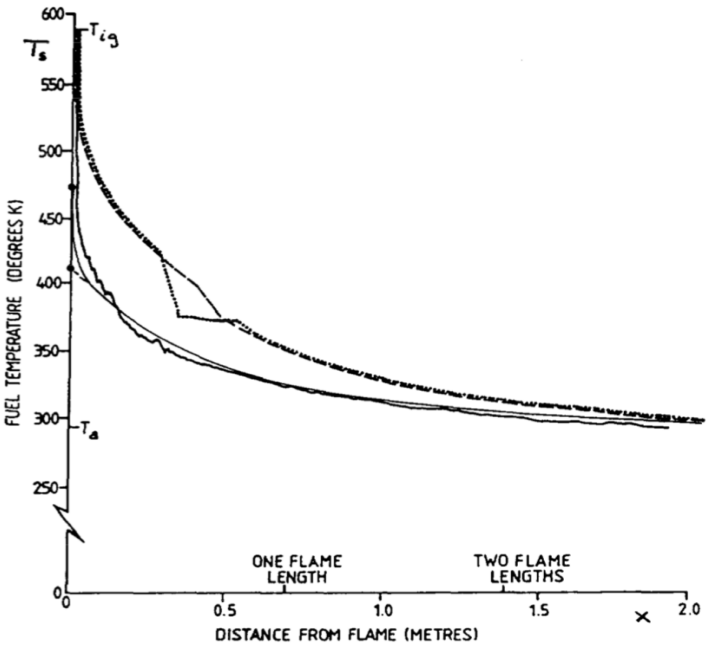


Figure 2.4.1: Fuel particle temperature: actual and modeled. The fine dashed line (model 1) has moisture evaporated at 373 K and the coarse dashed line (model 2) has continuously evaporated moisture complete at 373 K. but both represent radiation only models. The solid wavy line is the measured fuel temperature and the steady solid line is modeled fuel temperature with radiation and convection. (Graph from Baines 1990 [45])

This suggests that convective cooling from ambient air cools the fine fuels. Therefore, radiation alone may not be able to explain the ignition behavior of particles in fire spread. Experiments must be conducted to reveal how convective heating and cooling influence ignition. Flames carry hot and cold gases to contact fuel particles in fuel beds. When the fuel is heated by flame contact, it means the flame front extends and contacts the fuel. Factors such as flame frequency, and the duration of flame contact and the intermittent flame contact mechanism heats these fuels until it reaches ignition.

In wildland fires, radiation and convection play complementary roles. To better

predict the behavior of these fires it is necessary to understand the energy transport during these processes [27]. The extreme environmental conditions of wildland fires limits many measurement methods. Nonetheless, studies have reported the magnitude of radiative and total energy releases from wildland fires. Packham and Pompe reported radiative heat fluxes from slash fires in Australian forest lands [49]. Their work showed that the sensor type, orientation, and location relative to the fire significantly influenced measurements, in turn complicating comparisons between different tests.

In a study to better understand the effect of radiation and convection, Frankman et al. found that while measurable radiative heating occurred, convective cooling dominated energy transport in wildland fire spread before ignition [50]. The air drawn in to approaching flames convectively cooled the sensors as they were heated by the thermal radiation from the approaching flame. The tests were conducted on two sets of fuel types in a prescribed burn; sagebrush and a fuel type similar to a SG 10 fuel profile from Scott and Burgen [51]. The reported findings from their study stated that, with the approaching fire front, the radiative heating exhibited a gradual increase with a short and rapid rise right before ignition. Convective heating was characterized by an increase in heating pulses. This is a key indicator that the pulsation effect (flame intermittency) plays a role in the ignition of fine fuels with a thermally thin behavior. At ignition, it was seen that both radiative and convective heating contribute to this effect and likely depend on different fire regimes.

## 2.5 Types of fire spread models

Over the years, various wildland fire spread models have been developed to understand surface fire spread. Sullivan provided a comprehensive review of existing models between 1990 - 2007. [52, 53, 54]. Presented as three papers, the models were categorized into three groups: physical and quasi-physical models; empirical and quasi-empirical models; and simulation and mathematical analogous model.

Sullivan described a physical model as one that represents the physics and chemistry of fire spread [52]. A quasi-physical model represents only the physics aspect of spread. Empirical models contain no physical basis and are typically statistical in nature whereas a quasi-empirical model uses a physical framework on which the statistical model is based upon [53]. Empirical and quasi-empirical models can be further categorized into laboratory-based and field-based to differentiate fully controlled small-scale experiments conducted indoors and those that have limited control in the open.

Simulation models are those that implement a fire behavior model (often of low spatial dimensionality) in a landscape spread application thus addressing different sets of computation related problems [54]. Mathematical analogous are models those that utilize a mathematical precept rather than a physical one for the modelling of the spread of wildland fire.

From the 14 models discussed in the paper, Rothermel's fire spread model was listed as the primary spread model used in 9 of the predictive models reviewed by Sullivan. Computational fluid dynamic (CFD) models are generally three-dimensional, based

on the Navier-Stokes equations, the basic principles of fluid mechanics, heat transfer and conservation of mass, momentum and energy. Commonly used in areas of science and engineering, over the past two decades, CFD models have been adapted and applied to building fires and wildland fire problems. Currently, CFD based models are unable to provide a complete and accurate description relevant to fire dynamics [55]. Despite this, these models showcase a strong coupling between fire and the environment, often considered critical to a basic understanding of wildfire behavior. While some CFD-based models incorporate physically-based approaches to modeling fire spread, some use one-dimensional models like Rothermel at the fuel surface, further necessitating the need for a more comprehensive, physically-based model to be available.

## 2.6 Rubens Tube

In 1905, German physicists Rubens and Krigar-Menzel found a way to visually demonstrate acoustic standing waves behavior known as "flame tube", "standing wave flame tube" and "Rubens' tube". Because the Rubens' flame tube provides an exciting visual representation to better understand sound waves, it serves well as a teaching demonstration. Inspired by the works of Kundt who made the "Kundt tube" a tube filled with fine powder like cork dust and driven at resonance to identify the pressure anti-nodes once the dust settled [56]. Another precursor to the invention of the flame tube was a paper published by Behn in 1903 [57]. It described the sensitivity of flames to variations in ambient pressure. A combination of both the results led to

the development of this visually impressive device.

In this apparatus, flammable gas flows through the inside of the tube and then through the the small holes drilled along the top, and flames are lit above. The tube is closed at one end using a seal or casing and driven with a loud speaker at the other end. When audio is played at one of the tube's resonance frequencies, flames form a visual standing wave pattern and they vary in height according to the pressure amplitude of the tube as seen in figure 2.6.1.

Figure 2.6.1: A visual demonstration of standing wave using Rubens' tube

One of the most notable studies of the Rubens' Tube was performed by Ficken and Stephenson [58]. They showed that flame maxima occurred at pressure nodes within the tube and flame minima at the pressure anti-nodes. The results were explained using a simple model based on the incompressible Bernoulli equation indicating that the time averaged flow rate of the gas was greatest at the pressure nodes. However, for low gas flow rates, this effect reverses and the flame minima occurs at the pressure node and the flame maxima at the anti-nodes. Their work has offered the most complete explanation of the Rubens tube to date.

Jihui and Wang tried to understand the relationship between flame height and

pressure in the tube [59]. They reported that the flames were larger at the pressure anti-nodes and smaller at the pressure nodes which was a direct contrast to the works of Ficken and Stephenson. Due to the lack of information on gas pressure, it was difficult to tell. Spagna [60] focused on the behavior of the flame in the normal and reversal operation of the tube. He attempted to determine the relationship between the flicker in the flame to the speaker response. Using a Schileren projection of the flame, he observed banding in flames. The results were inconclusive in identifying a relationship. However, it was suggested that the flame and the standing waves may be decoupled where the flame is only probing the acoustic field inside the tube.

An extension of the original work done by Ruben, was that of Daw who created a square and circular flame table to visualize two-dimensional standing wave patterns [61, 62]. His work expanded on the different patterns observed and correlated it to better understanding flame structure in terms of eigen functions and a paper on visually demonstrating the acoustical modes in each hole.

Recent work by Gardner et al. [63], found that the holes on top of the tube were the primary cause of the shift in resonance frequencies. For a tube with larger holes (greater than 1 mm) the error shift came to 17% whereas for smaller tubes, it was 10%. The acoustic impedance in the hole is dependant on the frequency, playing a greater role at low frequencies than the higher ones. Depending on the parameters used to build the tube, this phenomena may or may not be strongly present. An implication from the study was measuring the wavelength of sound inside the flame tube using the flame pattern in conjunction with a definition for the speed of sound in the tube,

$$c = \lambda f \tag{2.1}$$

where $c$ is the speed of sound inside the tube [m/s], $\lambda$ the wavelength of sound [m] and $f$ the frequency [Hz].

In a more advanced setting, the tube can be used to better understand acoustical resonance behavior at a much deeper level. There are other likely uses for the flame tube, in understanding simple flame behavior under pressure and puffing characteristics.

## 2.7 Motivation

Development of a proper theory of how ignitions occur in wildland fires may aid in the development of an improved fire spread model in the future.As ignition is experimentally traceable, a solid physical theory can be developed for it in simplified configurations that represent real wildland fire scenarios. Previous models have incorporated processes of convection and radiation [13, 48], however the process of ignitions that occur at the fuel level have been assumed without sufficient experiments to verify these approaches. From the above literature review, numerous gaps in current knowledge can be found which motivate the present work.

The above summary points out several directions for further research. The present study aims to carry out research which will begin to address these gaps by focusing on intermittent heating and cooling of fine fuels by flames, incorporating both experiments and simple models which incorporate convective cooling.

# Chapter 3

# Experimental Apparatus and Instrumentation

## 3.1 Experimental Design

Stationary burners have been used to study fire spread in the built environment, focused on mean properties of the flame, but until recently have not been utilized for wildland fire or the study of intermittent flame effects on ignition. This research aims to understand and evaluate the effects of convection seen in wildland fires using a unique algorithm.

A pulsed-gas burner was designed for these experiments, shown in figure 3.1.1, recreating the pulsations observed in wildfires in a controlled laboratory environment. A 5 cm diameter, 40 cm long cylindrical aluminum tube is pressurized with propane gas at two inlets. A series of 31, 2 mm diameter holes with a separation distance of 0.5 cm are drilled in a line on the top of the cylinder, generating a relatively linear

flame front.

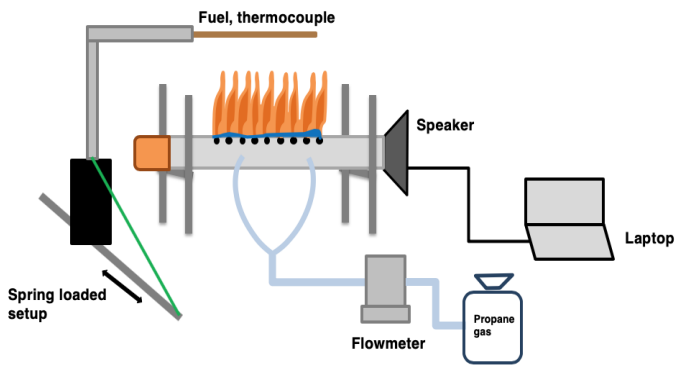


Figure 3.1.1: Experimental setup

Pulsations are generated via a speaker connected to one end of the tube, with pulses of increased amplitude causing pressure waves which produce intermittent bursts of flames above the device. The final design of the tube used for experiments is seen in figure 3.1.2

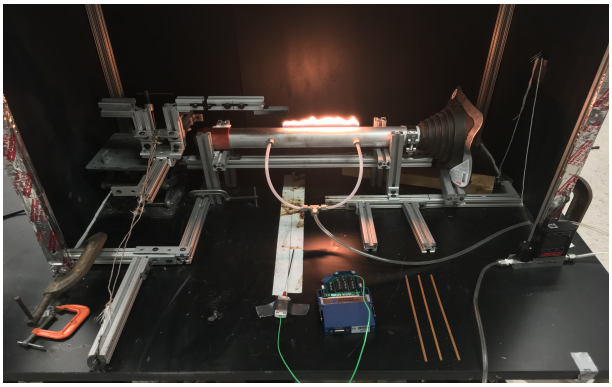

Figure 3.1.2: Experimental setup

Following preliminary testing, a sine wave of 200 Hz was applied and the audio was customized with varying amplitudes and duration of on and off times, to achieve the desired flame pulsation frequency. Pulsation frequencies are determined from a

Fast Fourier Transform (FFT) of temperature measurements in the plume, ranging from 0.5 - 5 Hz. Thin fuel elements made of basswood are used as fuel, due to their availability in varying sizes (0.08 cm, 0.16 cm and 0.32 cm). Ignition tests are conducted by quickly inserting the fuel into the center-line of the flame using a spring-loaded linear slider. By varying the flow rate of gaseous fuel and placing the fuel at different heights the temperature difference between the ambient and the peak temperature observed by the fuel element during a pulse could be varied between experiments.

Heating from the pulsating flame was also modeled using measured values and heat transfer correlations, assuming the elements are thermally thin from experimental results. Once it is assessed how various frequencies observed in wildland fire tests can relate to ignition and spread through diverse fuels, the framework can be used to quantify the influence of intermittent heating and cooling on fine fuel ignition. This could be applicable to wildland fire spread modeling in the future, once a simplified theoretical model for fuel ignition is developed based on the experiments.

## 3.2 Instrumentation and Software

A detailed description of the instrumentation and software used for data acquisition and analysis is given in the following section.

### 3.2.1 Digital Camera

A Nikon D7000 digital SLR camera (4,928  3,264 pixels) was used to capture flame side- view images during tests [Figure 3.2.1a]. In addition, a GoPro Hero 6 was used to capture a side-view video of the setup shown in figure 3.2.1b.


(a) Nikon D7000 [64]


(b) GoPro Hero 6 [65]

Figure 3.2.1: Digital cameras used during experiments

### 3.2.2 Thermocouple

To conduct tests and analyze the data, the temperature shifts of the flame at specified heights during tests had to be known as seen in figure 3.2.2.

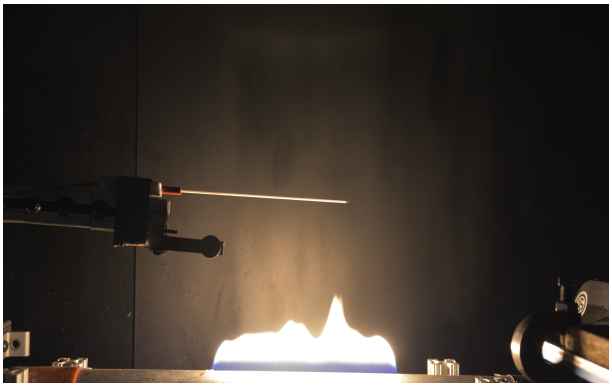

Figure 3.2.2: Thermocouple setup when used for temperature measurements

R-type thermocouples were used to capture this data. Wire diameters of 0.050 mm and 0.075 mm were used. The small diameter of the R-type thermocouple minimized thermal losses and decreased the lag time of the thermocouple. The response time of the thermocouple was estimated by the manufacturer to be on the order of 0.05 s. The small bead diameter also reduces disturbances to the flame and minimizes the radiation loss correction from thermocouple, estimated to be around 100 K at the maximum flame temperature measured [66]. A schematic of the thermocouple used is shown in figure 3.2.3.

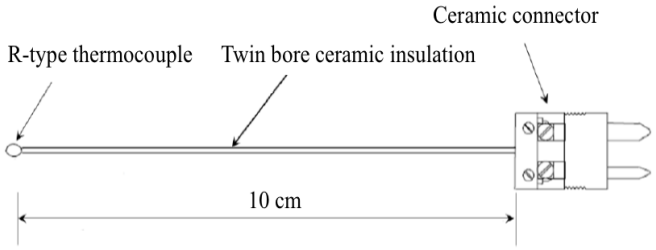


Figure 3.2.3: Thermocouple and mount used for temperature measurements

### 3.2.3 IR camera

An infrared camera, a FLIR E95 with a 7.5-14 $\mu$m spectral range, 640 x 480 pixel resolution, and 60 fps recording rate, is used to obtain a temperature profile of the stick as a function of time. The software used for this analysis is FLIR's Research IRMax. The software enables the user to adjust environmental parameters such as ambient temperature, emissivity, and distance from the object. The emissivity was set to 0.88 for all experiments [67].

While soot within the flame may distort temperature readings of the fuel surface

during pulsations, there is an adequate window with no flame present between pulses from which temperatures can be tracked to determine ignition times. These measurements will later be compared to fine wire thermocouple measurements on the fuel surface to verify the technique as a part of future work.

Figure 3.2.4 shows the setup of the camera, during an experiment, capturing data for ignition time analysis.

Figure 3.2.4: Thermocouple and mount used for temperature measurements

### 3.2.4 Data acquisition hardware and software

A Compact DAQ USB chassis with C-series I/O modules from National Instruments was used in experiments to record temperature measurements. For temperature measurements, the voltage signal from the thermocouple was acquired, conditioned and digitized through a NI 9214, which is a 24-bit high density 16-channel thermocouple input module with a 0.02°C measurement sensitivity. A built-in cold-junction compensation circuit is provided in the NI 9214. In addition to the cold-junction compensation system, the NI 9214 also has an extra, internal-only channel known as the auto-zero channel, from which an offset error can further be eliminated to provide more accurate measurements. The NI 9214 module is used

for thermocouple and heat flux measurements at high frequencies. For the duration of this work, a frequency response of 95 Hz on the card and 5 samples for every data collection cycle was set. LabVIEW is used for continuous data acquisition, with a script prepared to collect temperature measurements. The scripts also provide readings of the data, such as maximum value, minimum value, mean value and a real-time measure of the data being collected.

## 3.3 Measurement Methodology

Experiments were first conducted without any fuels, instead collecting temperature measurements using a fine-wire thermocouple. The frequency of pulsations, fuel flow rate, and the sampling distance from the burner were varied resulting in a large array of temperature measurements. By mapping the temperature difference between the peak temperature at the pulse and the ambient temperature between two pulses, the effects of distance, flow rate and flame frequency were studied. The same conditions were then used to identify ignition conditions where a fuel should be placed. In this case, the conditions to ignite the fuel using a minimal flow rate and the furthest distance from the burner were crucial in obtaining the maximum convective cooling and minimal radiation from the flame emanating from the burner between pulses. Once ignition with these conditions were obtained, thermocouples were placed to obtain the temperature difference, allowing for the dependence of ignition, fuel diameter and difference in temperature to be quantified.

### 3.3.1 Flame Velocity Measurements

Heat transfer correlations used to estimate heating from the flames are dependent on the flame temperature and velocity of the hot gaseous flowing. As intrusive diagnoses were not applicable of being used here, video footage was assessed to estimate the velocity of the flame. The flame itself was used as a flow tracker, shown in figure 3.3.1, where the flame tip as trailed as a function of time and the resulting distance travelled (red line) in addition to its instantaneous velocity (green line) is automatically calculated from the experiments conducted.

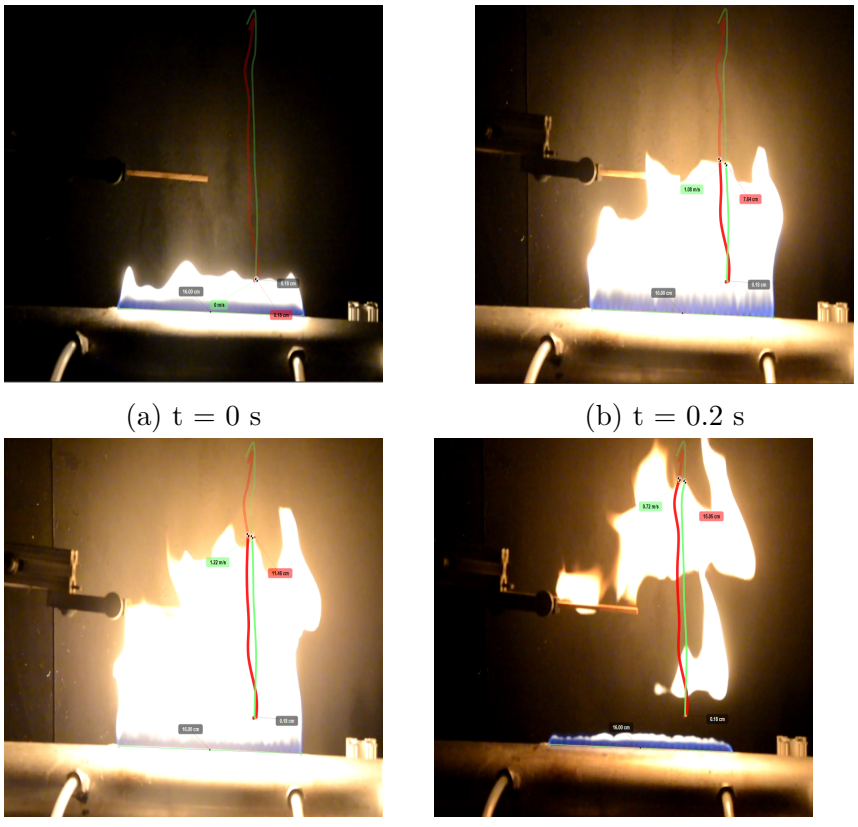

(a) t = 0 s (b) t = 0.2 s

(c) t = 0.25 s (d) t = 0.3 s

Figure 3.3.1: Flame velocity tracking using the software Kinovea

An enlarged image of the tracked path showing the distance the flame has traveled

and its velocity is seen in figure 3.3.2. The reference point taken to predict the values of velocity and distance is the length of the linear holes on the burner which was constructed to be 16 cm total in length. The initial height of the flame without any pulsations is observed to be around 0.18 cm by the software (Figure 3.3.3).

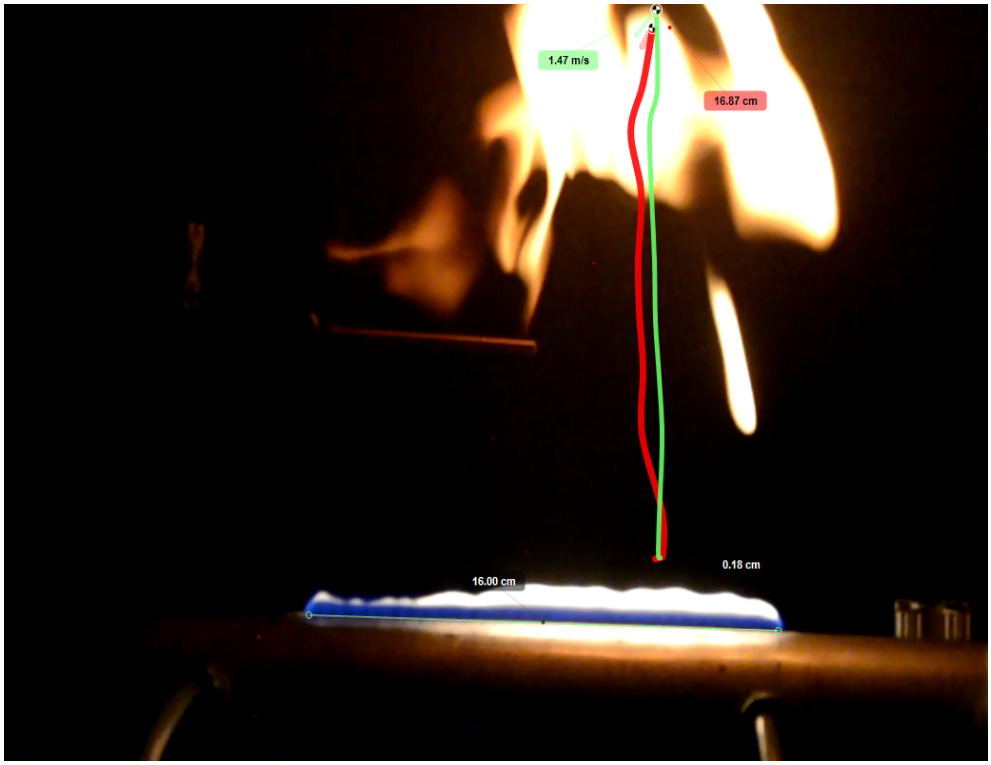


Figure 3.3.2: Represents the last point of the flame tracked

A simplified approach can also be used to estimate the velocity of the flame from equation 3.1.

$$v = \sqrt{gL} \tag{3.1}$$

where $g$ is the acceleration due to gravity (9.8 m/s$^2$) and $L$ is the length of the flame [m]. The plot showing representative velocities for different conditions is shown in figure 3.3.3 which are on the same order as those calculated from equation 3.1 for the

different heights of fuels studied.

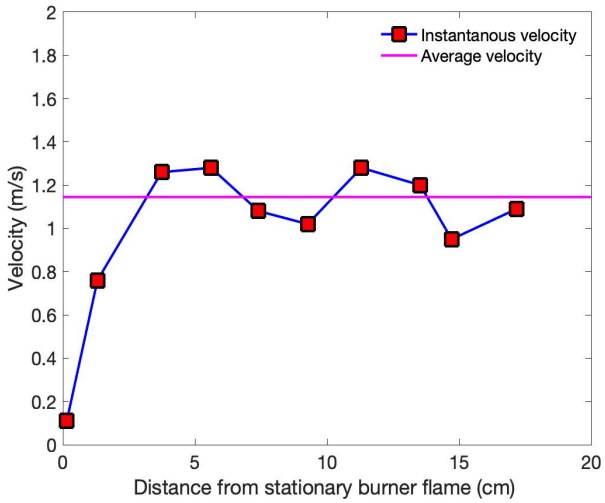


Figure 3.3.3: Represents the last point of the flame tracked

As shown, these velocities experience minor variations once the flame rises due to the audio pulsation which is after 2 cm from the stationary burner flame tip. The average velocity for the distances covered by the flame using the tracker was found to be 1.15 m/s.

## 3.4 Ignition test parameters

Understanding the ignition of fine fuels exposed to intermittent flames at varying frequencies is the basis of this study. These experiments are conducted with the previously-described gaseous burner varying the frequency of the flame, the size and type of fuels, as well as the location of the fuel, i.e. ignition on the center of the fine fuel versus the edge of the fuel . Figure 3.4.1a, 3.4.1b shows an ideal example when the center of the fuel is the ignition point (Center tests) and figure 3.4.1c, 3.4.1d

represent when the edge of the fuel is ignited.

(a) Image of a center test

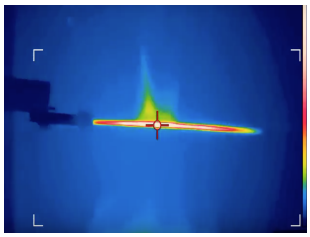

(b) IR image of a center test

(c) Image of an edge test

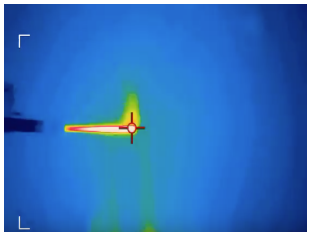

(d) IR image of an edge test

Figure 3.4.1: Visual difference between a center ignition test and an edge test

# Chapter 4

# Flame Characterization

## 4.1 Rubens' tube

In order to study the effects of intermittent heating on fuels, the first step was to characterize the flame. Originally, the Rubens' tube was used to show the relationship between sound waves and sound pressure. Music or audio generated through a speaker causes pressure waves to travel to the bottom of the tube, bounce back to the top of the tube and out the perforations. When propane gas fills the tube, it raises the internal pressure inside the tube greater than the atmospheric pressure as seen in figure 4.1.1. In this research, the tube is modified in an attempt to create large flame pulsations which mimic wildfire experiments.

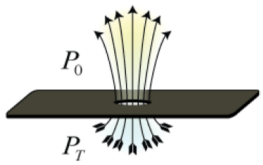


Figure 4.1.1: Inviscid flow through a hole [63]

Once a Rubens' tube is lit, the flames rise to a height related to the flow rate of the gas. If an assumption of inviscid and incompressible flow is used, the flow out of a perforation can be modelled using Bernoulli's equation. A simplification that considers the change in height of the fluid is negligible yields equation 4.1 [58],

$$\frac{\rho v^2}{2} = P_T - P_\infty \tag{4.1}$$

where $\rho$ is the density of the fluid [kg/m$^3$], $v$ the velocity of the ejected gas [m/s], $P_T$ is the pressure inside the tube and $P_\infty$ the atmospheric pressure.

Therefore, the velocity of the gas is proportional to the square root of the difference between the pressure within the tube and the atmospheric pressure [63].

$$v \propto \sqrt{P_T - P_\infty} \tag{4.2}$$

## 4.2 Audio file selection

In order to perform tests on fine fuels, a stable audio file had to be generated. The vital piece that enabled creating a sine wave audio file was the error sound used in a 2014 Macbook Pro. Using an audio editing software, Audacity, different parameters

such as frequency of the sine wave, amplitude, and time periods for on and off sections were varied to produce a steady flame frequency.

The sound introduced through the tube with the speaker was fixed as a sine wave. This was because sine waves not only helped create an optimal audio sound to run further experiments, but it also prevented the flame from extinguishing when played for long periods of time. Typically, the Rubens' tube uses music or audio from a frequency generator. The visual effects from the tube are also visually observed in the form of a sine wave but at 200 Hz the wave is barely visible and appears as standing flames [58].

The standing wave of the flame has a wavelength equivalent to that of the sound being played. The wavelength can be found using equation 4.3

$$\lambda = \frac{v}{f} \tag{4.3}$$

where $\lambda$ is the wavelength [m], $v$ the speed of sound through gas (approximately 258 m/s [68]) and $f$ the frequency generated [Hz].

Experimentally, the wavelength can be measured physically from peak to peak of the standing wave and verified using equation 4.2. However, for the purpose of this experiment, the number of holes on the tube was not sufficient to help visually identify the frequency played through the tube. It has been found that low frequencies played on the tube are difficult to identify from a visual standpoint [6].

To create a sine wave audio file to conduct experiments, the frequency had to be selected. Frequencies ranging from 10 Hz - 300 Hz were played for 0.1 seconds on the

speaker connected to the tube. The resulting flame effects were captured to find a frequency that resulted in break-off of the flame from the base of the tube that would mimic the intermittent region of a flame front. The result of the tests conducted are shown in table 4.1. Tests were conducted ten times to calculate the repeatability of flame break off which have been rounded off to the nearest tenth. A frequency of 200 Hz was found to be most suitable for the designed Rubens Tube as it always produced break-off in all experiments performed and therefore it was used to build the audio file.

Table 4.1: Frequency Selection

| **Frequency** (Hz) | **On Time** (s) | **Duration** (s) | **Result** | **Repeatability** (%) |
|---|---|---|---|---|
| 10 | 0.1 | 1 | No flame break off | - |
| 50 | 0.1 | 1 | No flame break off | - |
| 75 | 0.1 | 1 | No flame break off | - |
| 100 | 0.1 | 1 | No flame break off | - |
| 120 | 0.1 | 1 | No flame break off | - |
| 125 | 0.1 | 1 | Flame break off | 40 |
| 130 | 0.1 | 1 | Flame break off | 60 |
| 150 | 0.1 | 1 | Flame break off | 90 |
| 170 | 0.1 | 1 | Flame break off | 90 |
| 180 | 0.1 | 1 | Flame break off | 95 |
| 200 | 0.1 | 1 | Flame break off | 100 |
| 220 | 0.1 | 1 | Flame break off | 95 |
| 250 | 0.1 | 1 | Flame break off | 90 |
| 280 | 0.1 | 1 | Flame break off | 70 |
| 300 | 0.1 | 1 | Flame break off | 40 |
| 350 | 0.1 | 1 | No flame break off | - |

In order to find the total time duration of the flame (on and off time duration) equation 4.4 was used to obtain the total duration for a single wave packet (also known as a singular pulse) of a known frequency containing one specified on and off section (Table 4.2).

$$f = \frac{1}{T} \tag{4.4}$$

where $f$ is the frequency of the wave [Hz] and T the time period of the wave [s].

Table 4.2: Required time duration for each pulsation period according to frequency

| **Frequency** (Hz) | **Duration for single pulsation period**(s) |
|---|---|
| 0.1 | 10 |
| 0.2 | 5 |
| 0.3 | 3.33 |
| 0.4 | 2.5 |
| 0.5 | 2 |
| 1 | 1 |
| 2 | 0.5 |
| 3 | 0.33 |
| 4 | 0.25 |
| 5 | 0.2 |
| 8 | 0.125 |
| 10 | 0.1 |

### 4.2.1 On time

Intermittent heating effects seen in wildland fires have the flame coming in contact with the fuel for short periods of time. The typical flame frequencies observed in this region are between 0.5-10 Hz where time of flame contact is found to be lower than half a second from wildfire videos [5]. Experiments were conducted on the Rubens tube to identify the maximum time the flame can stay on for the duration's specified without extinguishing itself. The combination of the on-time and the specified off-time help create a well formed flame break off. Results from the tests are recorded in table 4.3. It was found that 0.1 s was the maximum time the flame could be "on".

Table 4.3: Selection of on-time duration

| **On Time** (s) | **Duration** (s) | **Result** |
|---|---|---|
| 0.05 | 1 | Flame sustained |
| 0.1 | 1 | Flame sustained |
| 0.2 | 1 | Flame extinguished |
| 0.3 | 1 | Flame extinguished |
| 0.4 | 1 | Flame extinguished |
| 0.8 | 1 | Flame extinguished |
| 1 | 1 | Flame extinguished |

### 4.2.2 Off time

Upon fixing the on time duration, an off time duration had to be fixed according to the frequency. By subtracting 0.1 seconds (on-time) from the total duration of a pulse period (Refer to Table 4.2) results in new off-time durations shown in table 4.4 with the necessary off time duration according to the required flame frequency.

Table 4.4: Required time duration for each pulsation period according to frequency

| **Frequency** (Hz) | **Duration for single pulsation period**(s) |
|---|---|
| 0.1 | 9.9 |
| 0.2 | 4.9 |
| 0.3 | 3.23 |
| 0.4 | 2.4 |
| 0.5 | 1.9 |
| 1 | 0.9 |
| 2 | 0.4 |
| 3 | 0.23 |
| 4 | 0.15 |
| 5 | 0.1 |
| 8 | 0.025 |
| 10 | 0 |

The combination of the on and off time duration of the signal creates a single pulse period. When this is repeated multiple times, it forms the audio file used in the

experiments.

### 4.2.3 Frequency measurement

Periodic pulsations observed in flames are one of the most visible characteristics observed by the human eye and has received considerable attention since 1950 [69]. Studies have shown that the pulsations are due to the periodic formation and, upward propagation of the vortices around a flame due to buoyant convection. A time dependent temperature reading (recorded at 95 Hz) was taken from a distance of 12 cm from the burner for intended frequencies at 0.5, 1, 2.5, 3.5 and 5 Hz. The collected readings were then converted to obtain the frequency of the pulsating flames using an FFT with the information of the audio files. The result, shown in figure 4.2.1, shows that the flame pulsates at the user specified frequency with almost no error. The interval between each peak in the graph provides the frequency of the flame. For example, for a 1 Hz audio file, the obtained FFT peaks were at 0.5 Hz, 1 Hz, 2.5 Hz, and so on.

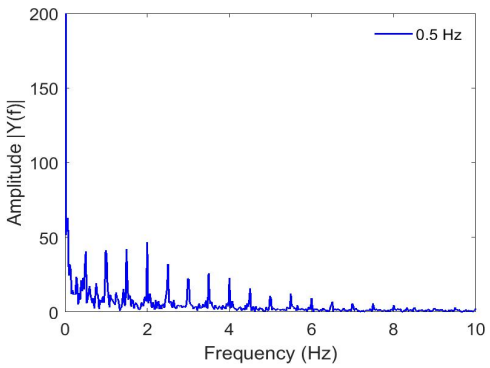


(a) 0.5 Hz

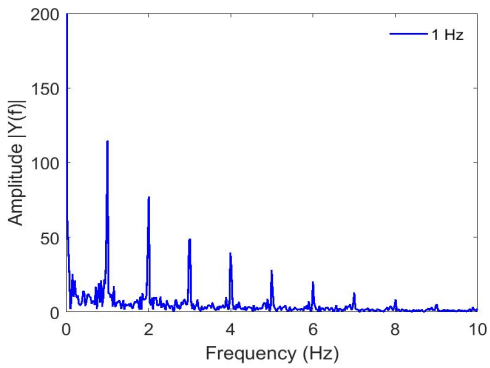


(b) 1 Hz

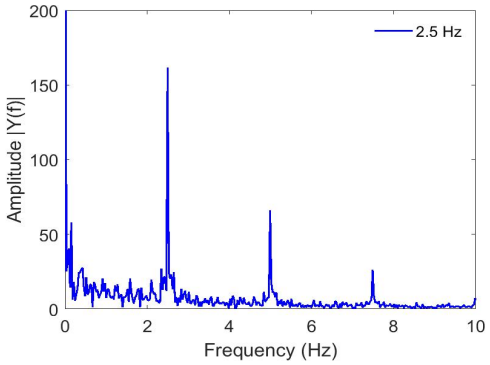


(c) 2.5 Hz

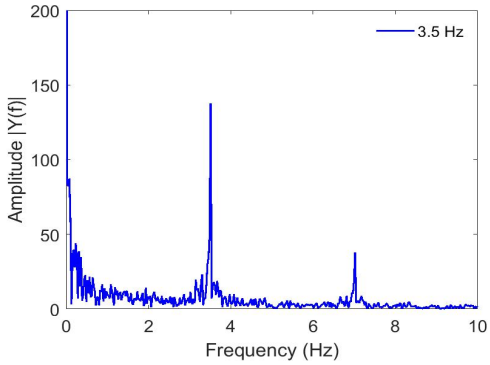


(d) 3.5 Hz

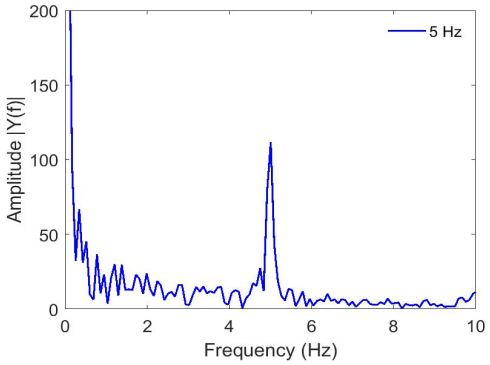


(e) 5 Hz

Figure 4.2.1: FFT results for different frequencies to verify flame frequency.

The key characteristics of the audio file for the five selected frequencies and the resulting flame frequencies from the thermocouple tests are noted in Table 4.5. Since the experimental flame frequencies are the same as the designed audio file, tests with different types of fine fuels were conducted to understand its effect on ignition.

Table 4.5: Selection of on-time duration

| **Frequency** (s) | **Duration of single pulse** (s) | | **Resulting FFT frequency** (Hz) |
|---|---|---|---|
| | **On Time** (s) | **Off Time** (s) | |
| 0.5 | 0.1 | 1.9 | 0.5 |
| 1 | 0.1 | 0.9 | 1 |
| 2.5 | 0.1 | 0.3 | 2.49 |
| 3.5 | 0.1 | 0.185 | 3.51 |
| 5 | 0.1 | 0.1 | 5 |

### 4.2.4 Temperature Profiles

Flames were characterized by placing an exposed R-type thermocouple (0.050 mm and 0.075 mm diameter) at pre-defined heights above the tube. Temperature measurements were taken at 95 Hz for several hundred pulsations over a period of time (30 seconds). Figure 4.2.2 shows the resulting temperature measurements for all flame frequencies tested for all experiments. A large $\Delta T$ was desired, therefore the sampling height and fuel flow rate was varied until an average peak value of 1030 K and a baseline value of 350 K was repeatably created at each frequency, resulting in a temperature difference of around 700 K with each pulse. For frequencies higher than 5 Hz, it was no longer possible to reach higher $\Delta T$ values, as cool air was unable to reach the test region in the time between between pulses. Variations in readings are mostly due to variability of the flame height, which may be caused by external factors such as ambient air flows in the laboratory and pressure differences within the tube. Additional variability is incorporated into these experiments due to the diverse nature of woody fuels, therefore tests are repeated numerous times, typically at least 10, to ensure a reasonable variability between all results.

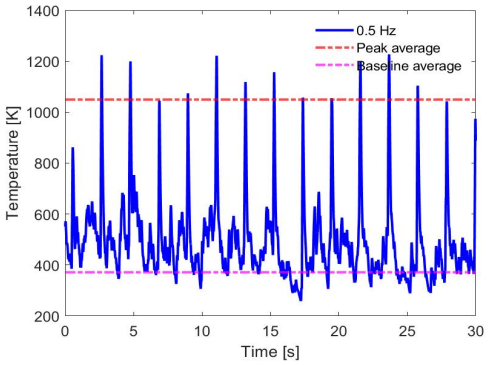


(a) 0.5 Hz

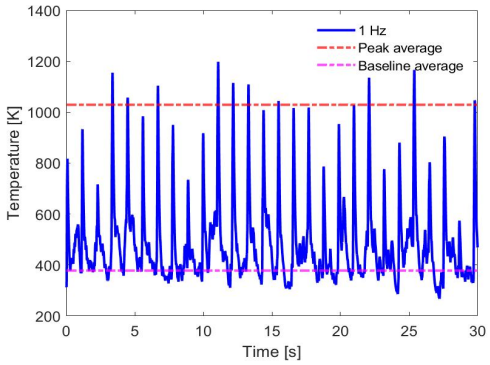


(b) 1 Hz

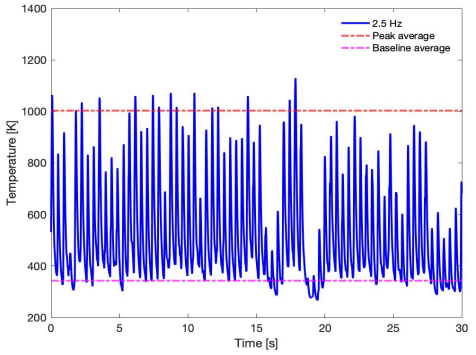


(c) 2.5 Hz

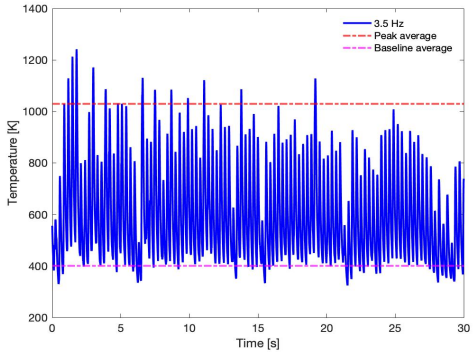


(d) 3.5 Hz

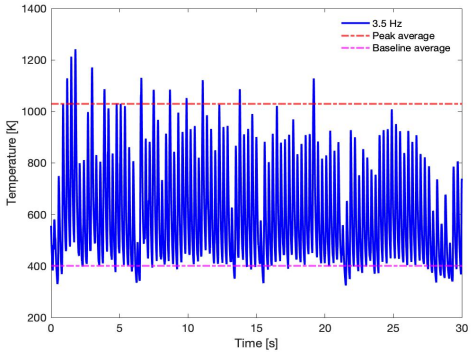


(e) 5 Hz

Figure 4.2.2: Temperature readings recorded above the burner for different applied frequencies. Gaseous fuel flow rates and the height of the fuel samples were adjusted in order to provide relatively similar temperature differences.

# Chapter 5

# Experimental Results

## 5.1 Fuel Characteristics

A variety of fuel types were selected to conduct ignition tests. These were selected based on both applicability and availability. The fuel characteristics and differences and base data used for each type of fuel are mentioned below.

Birch wood was selected as it's a common, easily-available wood product. Unfortunately, birch wood was not available in all desired sizes but 0.32 cm diameter samples were tested, a sample shown in figure 5.1.1.

Figure 5.1.1: Birch wood sample

Properties of birch wood from the literature are shown in table 5.1.

Table 5.1: Physical characteristics of birch wood

| **Variable** | **Value** |
|---|---|
| $\rho$ | 670.5 $\pm$ 97 kg/m$^3$ |
| $c_\mathrm{p}$ | 1.9 kJ/kgK [70] |
| $k$ | 0.14 W/mK [70] |
| $T_\mathrm{ig}$ | 575 K |
| $L$ | 19.5 cm |
| $d$ | 0.32 cm |

Basswood was available with the smallest dimensions, down to 0.08 cm, a sample stick shown in figure 5.1.2.

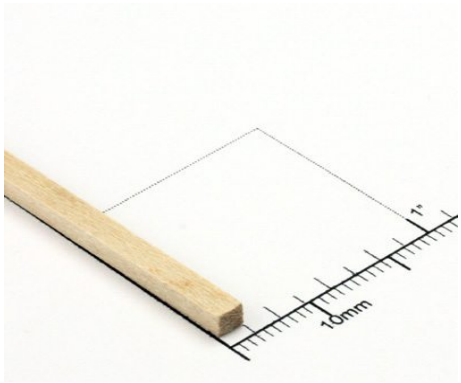


Figure 5.1.2: Basswood sample

Properties of basswood from the literature are shown in table 5.2.

In order to obtain the small scaled sticks square shaped was obtained, where cylindrical samples were previously used. Therefore, $d$ of basswood represents the width of any edge of a basswood square.

Properties of basswood used for calculations are shown in table 5.2.

Table 5.2: Physical characteristics of basswood

| **Variable** | **Value** |
|---|---|
| $\rho$ | 392 $\pm$ 150 kg/m$^3$ |
| $c_{\mathrm{p}}$ | 1.9 kJ/kgK [70] |
| $k$ | 0.14 W/mK [70] |
| $T_{\mathrm{ig}}$ | 573 K |
| $L$ | 20 cm |
| $d$ | 0.32 cm, 0.16 cm, 0.08 cm |

Pine needles were also tested as they represent a typical fine fuel in wildland fires. Dead long leaf pine needles were used as a part of this study (figure 5.1.3).

Figure 5.1.3: Pine needle samples

As a natural fuel, they experience a wide variation in dimensions and properties. Some values used from previous literature in this thesis are noted in table 5.3 .

Table 5.3: Physical characteristics of pine needle

| **Variable** | **Value** |
|---|---|
| $\rho$ | 270 ± 60 kg/m$^3$ |
| $c_\mathrm{p}$ | 1.5 kJ/kgK [70] |
| $k$ | 0.15 W/mK [70] |
| $T_\mathrm{ig}$ | 553 K |
| $L$ | 24.5 ± 3 cm |
| $d$ | 0.14 ± 0.02 cm |

Finally, hard paperboard used previously in experiments by Finney et al. were tested so that these samples could be assessed and compared from previous studies [5]. Their properties are shown in table 5.4.

Table 5.4: Physical characteristics of paperboard

| **Variable** | **Value** |
|---|---|
| $\rho$ | 600 ± 18 kg/m$^3$ |
| $c_\mathrm{p}$ | 1.7 kJ/kgK [70] |
| $k$ | 0.15 W/mK [70] |
| $T_\mathrm{ig}$ | 563 K |
| $L$ | 15 cm, 20 cm |
| $th$ | 0.25 cm, 0.1 cm |
| $d$ | 0.64 cm, 0.25 cm |

## 5.2 Visual analysis

An IR camera was used to record the experiments, as shown in figure 5.2.1.

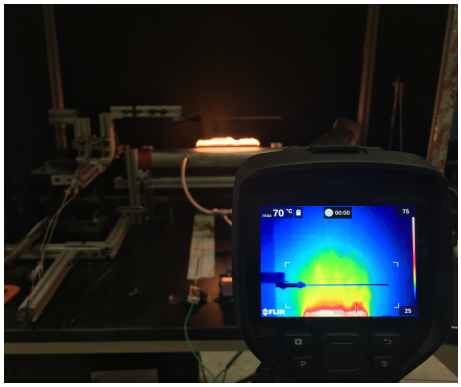

Figure 5.2.1: IR camera setup

The collected videos were then processed using proprietary FLIR software (IRMax) to obtain the temperature readings on the surface of the fuel throughout the experiment, an example shown in figure 5.2.2. The software allows changing factors such as emissivity, distance and other environmental conditions; however, because ignition occurs with a significant rise in temperature with respect to time, it is easy to note this threshold even if errors exist in temperature readings.

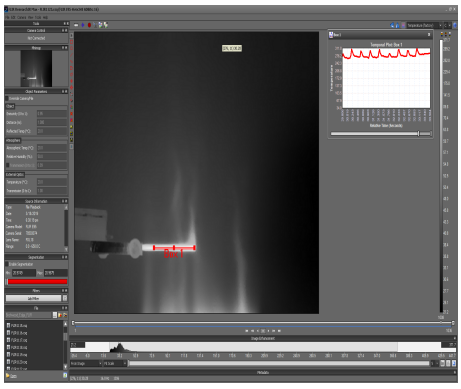

Figure 5.2.2: Gathering surface temperature data from software IRMax

An example of recorded temperature data is shown in Figure 5.2.3 for a scenario where a sample ignites and one where it is heated but does not achieve ignition. A

basswood stick of diameter 0.16 cm was used here, exposed to a flame frequency of 1 Hz at 9 and 12 cm from the burner, creating different temperature differences of 700 K and 850 K which affected the ability of the stick to ignite.

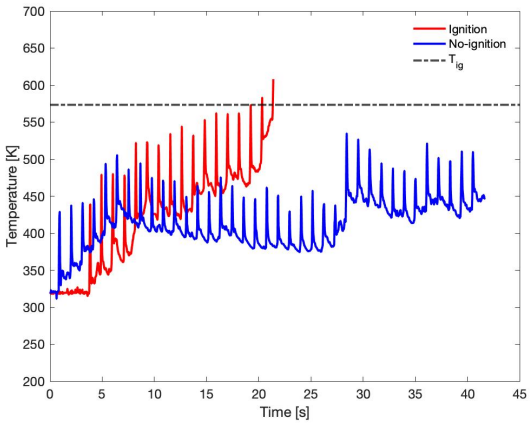


Figure 5.2.3: Raw temperature measurements taken from IR readings are shown for two samples where pulsations of the flame distort the surface temperatures of the fuel

Temperature data from the IR camera is later processed to remove temperatures where the flame is present between the camera and the fuel sample using a MATLAB code incorporating the 'envelope' function that follows the base temperature values, resulting in a smoother line that more accurately represents the temperature of the fuel surface as seen in figure 5.2.4.

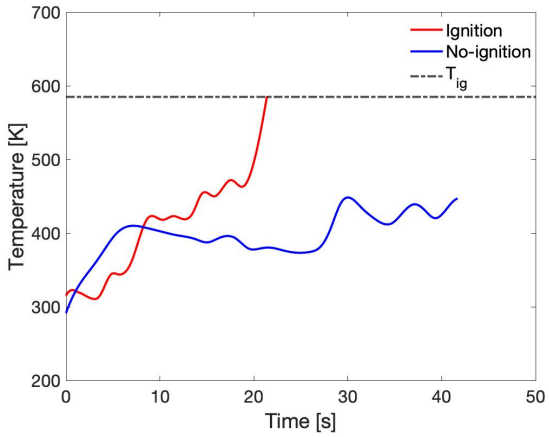


Figure 5.2.4: Surface temperature measurements taken from IR readings are shown for a sample that ignites and one that is heated but does not ignite.

## 5.3 Ignition conditions

Experiments were conducted to understand if there was any plausible effect on ignition time with respect to flame frequencies. Standardizing the tests to minimize the number of variable parameters was vital. This was done by running tests in the similar environment conditions at all times, fixing the burner distance (testing height) that would have similar temperature differences with change in frequency and using similar gas flow rates. As frequency increased, the testing height was observed to increase so that the temperature difference ($\Delta T$) remained around the 700 K mark. The resulting ignition times were identified and the mean value over 10-15 successful tests were used for analysis. In addition to this, tests were conducted to identify the furthest distance from the burner where ignition still occurred and named as "limit height" for the remainder of the document. This indicated the presence of an ignition and no-ignition zone that was dependent on the temperature difference and distance

from the burner. It should be noted that testing and limit height is identified as the distance of the fuel from the top of the burner in centimeters. The following section discusses the different observations found from the experiments. A detailed analysis on each of these effects is done in the following sections.

### 5.3.1 Birch

Birch wood, one of the thickest fuels tested, showed a decrease in ignition time with increase in flame frequency. At the slower pulsations (0.5 - 1 Hz) the ignition time varies quite extensively due to the unpredictability of the flame hitting the stick at random locations and varying intensities. This called for more tests to be conducted in order to better represent the data and eliminating any outlier. This variability in flame contact reduces with higher frequency, also reducing the ignition times drastically as seen in figure 5.3.1.

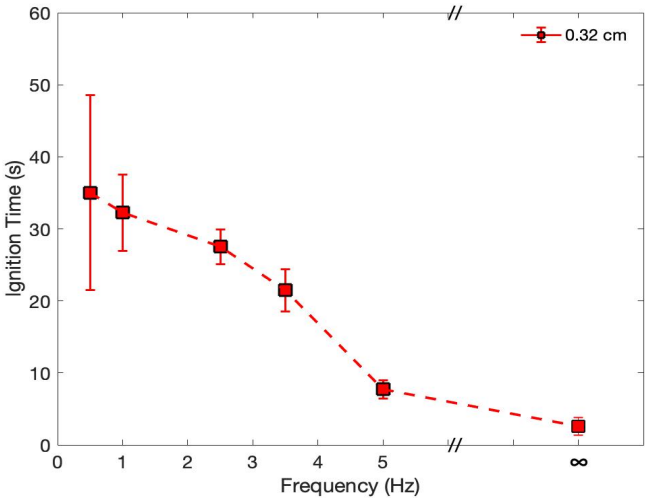


Figure 5.3.1: Ignition times for birch wood heated at the center for different frequencies

For a 0.5 Hz, center test, ignition occurs around the 35 seconds mark and experiments show that the stick ignites within 8 seconds with a 5 Hz flame frequency. It indicates that the intermittency of the flame plays a significant role in ignition. Being a relatively thicker fuel, the testing height with higher frequencies only increased by a few centimeters (Table 5.5. Similar effect was seen with its ignition limit height although the limit heights increase more with higher frequencies (notable after 3.5 Hz). The resulting ignition times at the testing height where temperature difference was fixed at $\Delta T$ around 700 K are shown in table 5.5 for center tests and table 5.6 for edge tests. The maximum distances from the burner where ignition is possible have been noted in table 5.5 for center tests and table 5.6 for edge tests.

Table 5.5: Birch wood - Center

| **Frequency** (Hz) | **Testing Height**(cm) | **Mean Ignition time**(s) | **Limit Height**(cm) |
|---|---|---|---|
| 0.5 | 10 | 35 ± 13.5 | 10 |
| 1 | 10.5 | 32.2 ± 5.32 | 10.5 |
| 2.5 | 11 | 27.5 ± 2.4 | 11.5 |
| 3.5 | 12.5 | 21.46 ± 2.9 | 13 |
| 5 | 13.5 | 7.71 ± 1.25 | 15 |

Comparing the results between the center and edge tests of Birch wood shows that while edge tests ignite faster (2 - 5 seconds), changes in the height from the burner doesn't result in drastic variations in ignition time (figure 5.3.2). This is due to the thicker diameter of the fuel, resulting in a lower SAVR as compared to the other fuels tested, thus being less sensitive to the intermittency of the flame.

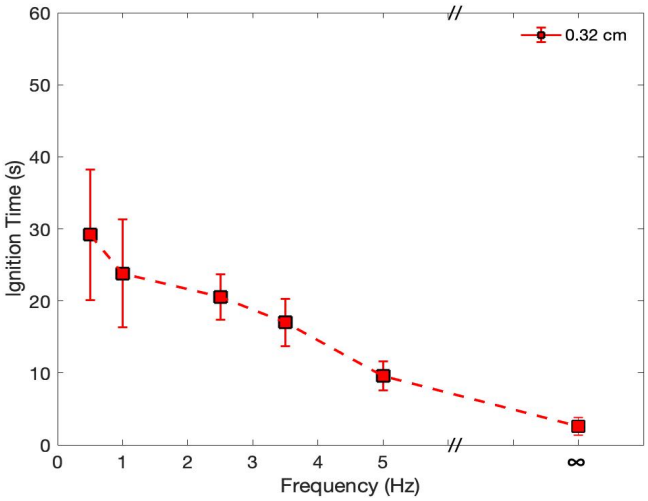


Figure 5.3.2: Ignition times for birch wood heated at the edge for different frequencies

Table 5.6: Birch wood - Edge

| **Frequency** (Hz) | **Testing Height**(cm) | **Mean Ignition time**(s) | **Limit Height**(cm) |
|---|---|---|---|
| 0.5 | 10 | 29.2 ± 9 | 10 |
| 1 | 10.5 | 23.8 ± 7.5 | 11 |
| 2.5 | 11 | 20.5 ± 3.16 | 11 |
| 3.5 | 12 | 17 ± 3.27 | 13 |
| 5 | 13 | 9.56 ± 2.02 | 14 |

Another observation noted is that the testing heights are fairly close to the limit region of ignition indicating that fuels with a diameter greater than 0.4 cm would be less likely to ignite when exposed to these flame pulsations.

### 5.3.2 Basswood

Ignition tests were conducted on basswood sticks with a thickness of 0.08 cm, 0.16 cm and 0.32 cm for flame frequencies of 0.5 Hz, 1 Hz, 3 Hz and 5 Hz. The relationship between the thickness of the stick, frequency and ignition times were studied. The

effect of temperature differences was also studied, and is presented in a later section. Tests were also conducted for a constant flame (representing a high frequency). The resulting trends are plotted with their respective standard deviation between repeated tests in Figure 5.3.3. Basswood has the largest variation in terms of fuel thickness (0.08 cm, 0.16 cm and 0.32 cm). Results from these tests have shed more light on how fuel thickness plays a role and reacts differently to the flame pulsations.

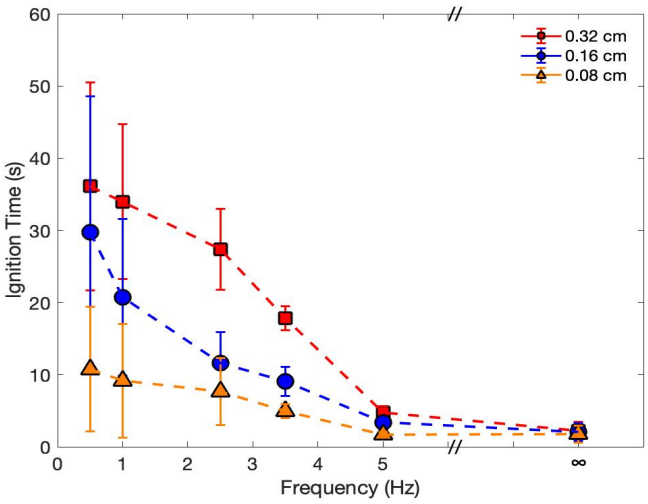


Figure 5.3.3: Ignition times for basswood sticks heated in the center at different frequencies with a fixed $\Delta$T of 700 K

Table 5.7: Basswood - Center

| **Diameter** (cm) | **Frequency** (Hz) | **Testing Height** (cm) | **Mean Ignition time** (s) | **Limit Height** (cm) |
|---|---|---|---|---|
| **0.32 cm** | 0.5 | 10 | 36.1 ± 14.4 | 11 |
| | 1 | 10.5 | 34 ± 10.75 | 11 |
| | 2.5 | 10.5 | 27.4 ± 5.6 | 12 |
| | 3.5 | 10.5 | 17.8 ± 1.7 | 14 |
| | 5 | 11 | 4.75 ± 0.89 | 17 |
| **0.16 cm** | 0.5 | 10 | 29.7 ± 18.9 | 12 |
| | 1 | 10.5 | 20.7 ± 10.9 | 13 |
| | 2.5 | 11.5 | 11.7 ± 4.3 | 15 |
| | 3.5 | 12.5 | 9.06 ± 2 | 16 |
| | 5 | 13 | 3.4 ± 0.5 | 17 |
| **0.08 cm** | 0.5 | 12 | 10.76 ± 8.65 | 13 |
| | 1 | 12.5 | 9.18 ± 7.89 | 13 |
| | 2.5 | 13 | 9.67 ± 4.66 | 15 |
| | 3.5 | 14 | 4.95 ± 0.95 | 18 |
| | 5 | 15 | 1.7 ± 0.35 | 24 |

The thickest size, 0.32 cm, follows a very similar trend to birch wood of the same thickness as shown in figure 5.3.4.

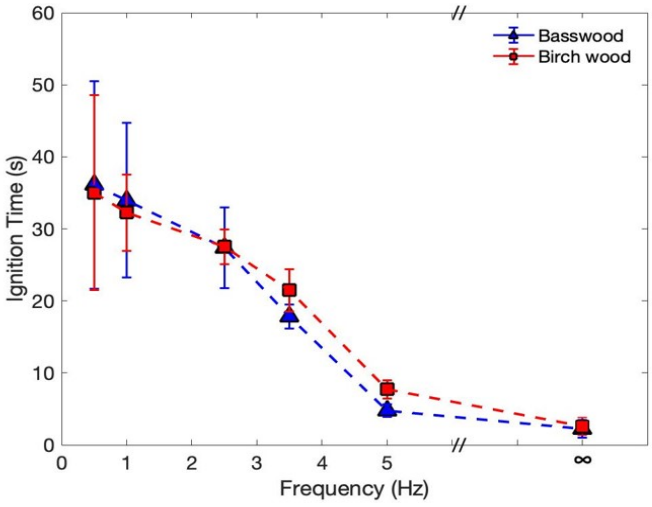


Figure 5.3.4: Ignition times for basswood and birch wood stick of size 0.32 cm heated at different frequencies with a fixed $\Delta$T of 700 K

With the exception of shape and density of different fuels forming some small differences, overall basswood and birch wood respond to intermittent heating similarly. Like previous observations, the ignition time reduces with an increase in flame frequency and the variability is greater at lower frequencies.

The mid-sized fuel, with a thickness of 0.16 cm, has a lower ignition time than its thicker counterpart. The increase in SAVR and a more thermally thin behavior accelerates the temperature of the stick with each pulsation causing quicker ignition. The thinnest Basswood stick, 0.08 cm, has a slightly unique behavior than the other sizes. The higher SAVR causes the stick to reach ignition with very few pulses. While the variations in ignition times at lower frequencies still exist, the stick, due to its thin nature, has a larger variability in ignition time requiring a minimum of 15 tests to average the results. The smaller difference in ignition time indicates that the thinner fuels aren't affected by the flame intermittency and location of the stick exposed to the flame (figure 5.3.5) as significantly as the thicker fuels.

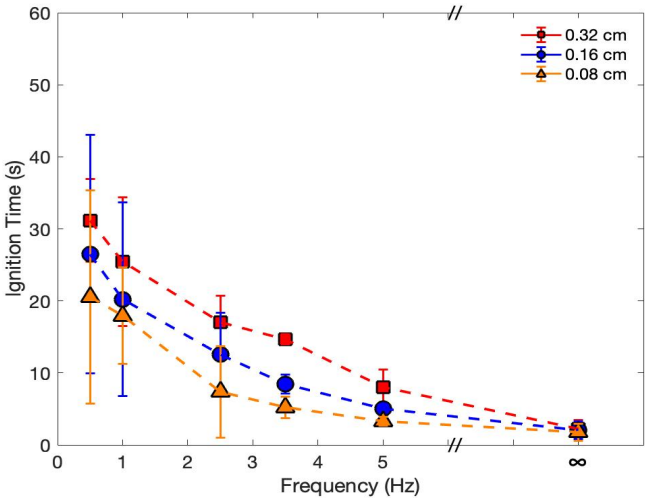


Figure 5.3.5: Ignition times for basswood sticks heated in the edge at different frequencies with a fixed $\Delta$T of 700 K

Comparing all the three sizes of fuel together, it is noted that the height at which fuel were tested to have a temperature difference of 700 K (testing height) and the furthest distance where ignition occurs (limit height) increases quickly with a decrease in thickness when data from tables 5.7 and 5.8 are compared.

Table 5.8: Basswood - Edge

| **Diameter** (cm) | **Frequency** (Hz) | **Testing Height** (cm) | **Mean Ignition time** (s) | **Limit Height** (cm) |
|---|---|---|---|---|
| **0.32 cm** | 0.5 | 10 | 31.15 ± 5.8 | 10 |
| | 1 | 10.5 | 25.45 ± 8.9 | 11 |
| | 2.5 | 10.5 | 17.03 ± 3.6 | 11 |
| | 3.5 | 10.5 | 14.65 ± 0.68 | 12 |
| | 5 | 11 | 8.03 ± 2.5 | 13 |
| **0.16 cm** | 0.5 | 10 | 26.47 ± 16.5 | 12 |
| | 1 | 10.5 | 20.23 ± 13.45 | 12 |
| | 2.5 | 11.5 | 12.55 ± 5.78 | 14 |
| | 3.5 | 12.5 | 8.45 ± 1.32 | 15 |
| | 5 | 13 | 5.03 ± 0.37 | 16 |
| **0.08 cm** | 0.5 | 12 | 20.55 ± 14.8 | 15 |
| | 1 | 12.5 | 17.95 ± 6.68 | 17 |
| | 2.5 | 13 | 7.38 ± 6.33 | 17 |
| | 3.5 | 14 | 5.23 ± 1.48 | 19 |
| | 5 | 15 | 3.3 ± 0.58 | 22 |

### 5.3.3 Pine needles

Dried pine needles from longleaf pine, the thinnest fuel type tested, showed behavior similar to 0.08 cm diameter Basswood sticks as seen in figure 5.3.6. With ignition times reducing as frequency increased, pine being a natural fuel had a lot of variations in terms of its length, thickness and shape. This in turn slightly affected the tests and results.

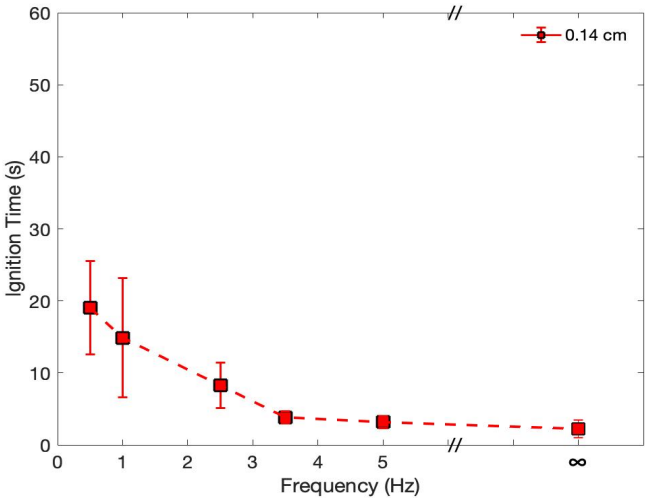


Figure 5.3.6: Ignition times for pine needle heated at the edge for different frequencies

Overall, the fuel being thin results in behavior that is thermally thin in nature. The limit heights increased drastically as compared to the previous fuel (Table 5.9), showing that an intermittent flame is capable of igniting the fuel from a distance of 15 cm away, greater than other fuels tested.

Table 5.9: Pine needle - Center

| **Frequency** (Hz) | **Testing Height**(cm) | **Mean Ignition time**(s) | **Limit Height**(cm) |
|---|---|---|---|
| 0.5 | 13 | 19.02 ± 6.5 | 14 |
| 1 | 13 | 14.9 ± 8.3 | 14 |
| 2.5 | 13.5 | 8.3 ± 3.11 | 15 |
| 3.5 | 14 | 3.83 ± 0.83 | 16 |
| 5 | 15 | 3.16 ± 0.86 | 21 |

### 5.3.4 Paperboard

Experiments were performed on a slightly different material of two different thickness, 0.64 cm and 0.25 cm, to understand if combs of paper-based fuel would experience

the same behavior as woody fuels. It should be noted that the paperboard used are the same ones from experiments conducted by Finney et al. [6]. Results indicate that they do follow the same trend lines in testing heights, ignition time and limit heights as seen in figures 5.3.7, 5.3.8 and tables 5.10 and 5.11. A unique factor seen during tests is that the cardboard tends to pyrolyze or smolder in the beginning prior to ignition.

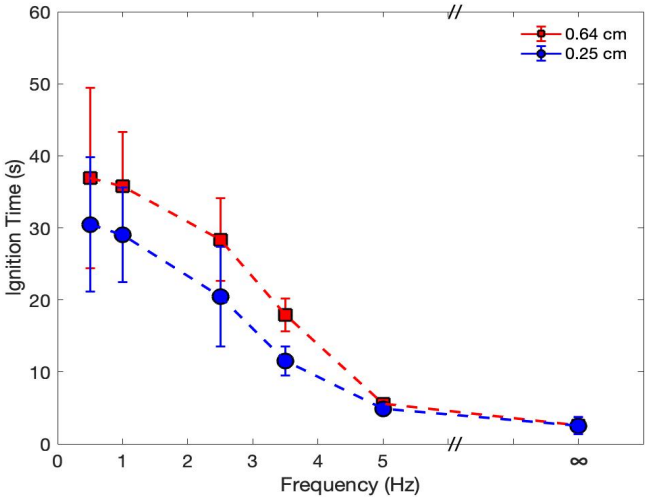


Figure 5.3.7: Ignition times for cardboard sticks heated in the center at different frequencies

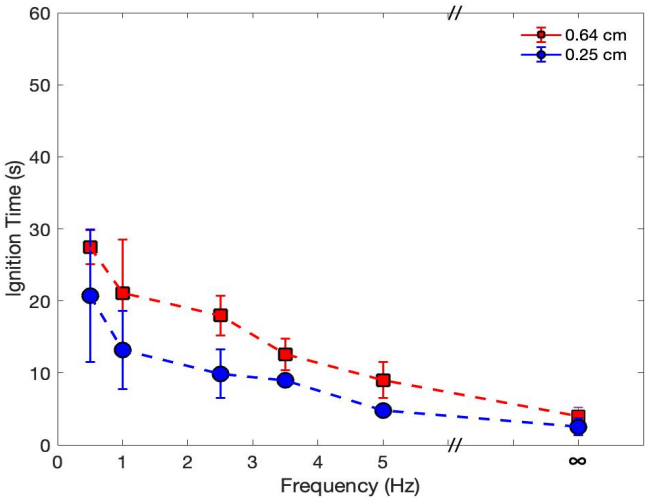


Figure 5.3.8: Ignition times for cardboard sticks heated at the edge for different frequencies

While the ignition time reduces with frequency, the rate of reduction in this fuel type is slower and more gradual than basswood and birch wood. This could be due to the difference in the fuel characteristics like molecular structure and other chemical properties.

Table 5.10: Paperboard - Center

| **Diameter** (cm) | **Frequency** (Hz) | **Testing Height** (cm) | **Mean Ignition time** (s) | **Limit Height** (cm) |
|---|---|---|---|---|
| **0.64 cm** | 0.5 | 9.5 | 37 ± 12.5 | 11 |
| | 1 | 10 | 35.7 ± 7.5 | 11 |
| | 2.5 | 10 | 28.4 ± 5.7 | 12 |
| | 3.5 | 10.5 | 18 ± 2.2 | 14 |
| | 5 | 11 | 5.6 ± 0.5 | 17 |
| **0.25 cm** | 0.5 | 12 | 30.5 ± 9.34 | 12 |
| | 1 | 12.5 | 29 ± 6.6 | 13 |
| | 2.5 | 13 | 20.5 ± 6.93 | 15 |
| | 3.5 | 13 | 11.5 ± 2.03 | 16 |
| | 5 | 14 | 4.5 ± 0.45 | 17 |

Table 5.11: Paperboard - Edge

| **Diameter** (cm) | **Frequency** (Hz) | **Testing Height** (cm) | **Mean Ignition time** (s) | **Limit Height** (cm) |
|---|---|---|---|---|
| **0.64 cm** | 0.5 | 9.5 | 27.5 ± 2.4 | 11 |
| | 1 | 10 | 21.1 ± 7.5 | 12 |
| | 2.5 | 10 | 17.9 ± 2.8 | 13 |
| | 3.5 | 10.5 | 12.6 ± 2.2 | 14 |
| | 5 | 11 | 8.99 ± 2.5 | 16 |
| **0.25 cm** | 0.5 | 12 | 20.8 ± 9.2 | 13 |
| | 1 | 12.5 | 13.2 ± 5.5 | 14 |
| | 2.5 | 13 | .86 ± 3.4 | 17 |
| | 3.5 | 13 | 8.9 ± 0.7 | 17 |
| | 5 | 14 | 4.8 ± 0.35 | 20 |

## 5.4 Constant flame

An analysis was performed in order to identify if the sticks could be assumed to behave as thermally thick or thermally thin materials using equation 5.1 [71],

$$\frac{t_w}{t_p} = \frac{\dot{q_{in}}'' \, d}{k(T_p - T_i)} \tag{5.1}$$

where $t_w$ is the time of thermal wave propagation [s], $t_p$ is the time for the stick to pyrolyze and ignite [s], $\dot{q_{in}}''$ is the heat flux from the flame to the stick [W/m$^2$], $d$ is the thickness of the stick [m], $k$ the thermal conductivity of wood [W/mK], $T_p$ is the pyrolysis temperature [K], and $T_i$ the initial temperature of the stick [K].

If $t_w/t_p < 0.1$, a material is usually assumed thermally thin, without internal temperature gradients being considered. From calculations, all the basswood sticks were found to be close to thermally thin. The theoretical time to reach a heat of pyrolysis for thermally thin elements was then calculated [71],

$$t_p = \frac{\rho c_p \ (T_p - T_i) \ d}{\dot{q_{in}}''} \tag{5.2}$$

where $t_p$ is the time for the stick to pyrolyze and ignite [s], $\rho$ is the density of the stick [kg/m$^3$], and $c_p$ is the specific heat capacity of the wood [kJ/kg K].

The heat transfer coefficient is found by calculating $Nu$, the Nusselt number, using equation 5.3 [71].

$$h = \frac{Nu \quad k}{L_c} \tag{5.3}$$

For a low Reynolds number and $Pr > 0.6$ [47],

$$Nu_D = 1.15 Re_D^{1/2} Pr^{1/3} \tag{5.4}$$

where $Nu_D$ is the Nusselt number, $Re_D$ is the Reynolds number and $Pr$ is the Prandtl number of air.

Alternatively, the Biot number can be calculated for the three sizes of wood,

$$Bi = \frac{hL_c}{k} \tag{5.5}$$

where $h$ is the heat transfer coefficient [W/m$^2$K], $L_c$ the characteristic length, which is commonly defined as the volume of the body divided by the surface area of the body and $k_b$ the thermal conductivity of the body [W/mK]. The Biot number for sticks of sizes 0.32, 0.16 and 0.08 cm were 0.36, 0.26 and 0.19, respectively, roughly

maintaining a thermally-thin assumption. If $Bi << 1$, convective heat transfer to the surface is significantly slower than internal conduction heat transfer. What results is no significant temperature variation inside the body, implying that temperature gradients can be ignored, allowing a lumped capacitance model to be used. However, results show that these fuels lie roughly near, but not entirely in the thermally-thin regime, meaning that while taking that assumption in analysis may work reasonably well for smaller diameters, additional errors will be introduced as the diameter of the fuels increases.

The resulting ignition times were calculated and compared to experimental values for tests using a constant flame (no pulsations). Figure 5.4.1 provides a plot of the resulting 'steady' ignition times for the basswood sticks of three different sizes.

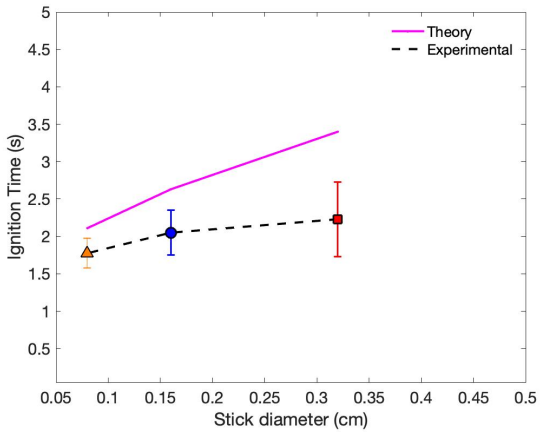


Figure 5.4.1: Theoretical and experimental ignition times for basswood sticks exposed to a constant flame.

Figure 5.4.1 and table 5.12 shows that the theoretically-calculated ignition times roughly, for basswood, follow the same trends up to 0.16 cm, increasing in time with increasing diameters.

Comparing all the ignition times for the different fuel types, shown in figure 5.4.2, it can be seen there is a lot of variability and difference in prediction between theory and experiments.

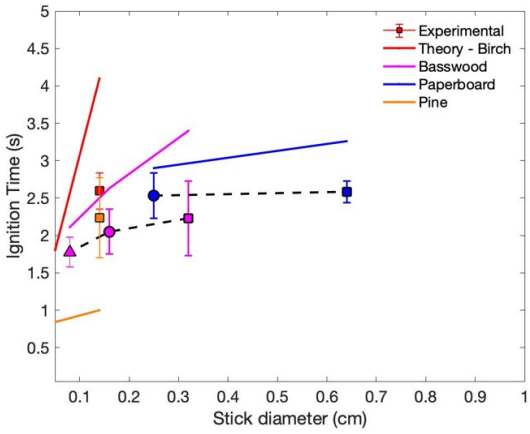


Figure 5.4.2: Theoretical and experimental ignition times for all fuels exposed to a constant flame.

The predicted ignition times are typically higher than the experimental results, possibly due to variations in the flame over time, variability in the wood and its properties, and numerous assumptions incorporated into this simplistic analysis, notably an assumption of lumped capacitance due to the fuels small diameter. The difference increases with increasing stick diameter, which also suggests the thermally-thin assumption may not be accurate for all sizes. The under-prediction of ignition time for pine needles is partly due to inaccuracy in obtaining ignition times from experiments using the FLIR software. Being a natural fuel, the dimensions varied more than the other fuel types. More tests will be conducted in the future to determine the accuracy of these assumptions.

Table 5.12: Constant flame for all materials

| **Wood** | **Thickness**(cm) | **SAVR** ($cm^{-1}$) | $t_{ig,exp}$ (s) | $t_{ig,theory}$(cm) | **Bi** |
|---|---|---|---|---|---|
| **Birch** | 6.25 | 0.32 | 2.6 ± 0.24 | 4.1 | 0.36 |
| **Basswood** | 0.32 | 12.6 | 2.23 ± 0.42 | 2.12 | 0.36 |
| | 0.16 | 25.1 | 2.05 ± 0.23 | 1.62 | 0.26 |
| | 0.08 | 50.1 | 1.77 ± 0.15 | 1.3 | 0.19 |
| **Cardboard** | 0.64 | 6.4 | 2.58 ± 0.14 | 3.88 | 0.30 |
| | 0.25 | 16.1 | 2.53 ± 0.3 | 1.85 | 0.20 |
| **Pine** | 0.06 | 14.3 | 2.23 ± 0.54 | 0.7 | 0.23 |

### 5.4.1 Summary of ignition time results

The mean ignition time for sticks of all thicknesses decreases as a function of increased flame pulsation frequency. As expected, the smaller the thickness of the stick, the shorter the ignition time. Frequency, however, plays a greater role with larger thickness sticks. This highlights how heating and cooling, due to the intermittency of the flame, depends on the thickness or diameter of fuels. For thicker fuels, the cooling period between pulses allows for convective cooling, preventing it from reaching the ignition temperature. If the stick is unable to reach this point, it cannot produce enough pyrolyzate to sustain ignition and either internally chars or extinguishes at the end of every pulse. Very fine fuels with a high surface area to volume ratio respond very effectively to each pulse, reaching an ignition quickly.

In a wildland fire, where very fine fuels are often the medium supporting the progression of the flame front, this shows that intermittent heating may only provide a slight delay in ignition times.

## 5.5 Temperature dependence on ignition

After running multiple experiments to identify the effect of ignition time across various flame frequencies at a fixed temperature difference, the influence of these temperature difference on ignition was studied as shown in figure 5.5.1. By varying the distance from the burner for varying flame frequencies ranging from 0.5 - 5 Hz, resulting in ignition, thermocouple measurements were collected from the furthest distance from the burner. The difference in temperature for each test was identified and plotted as follows.

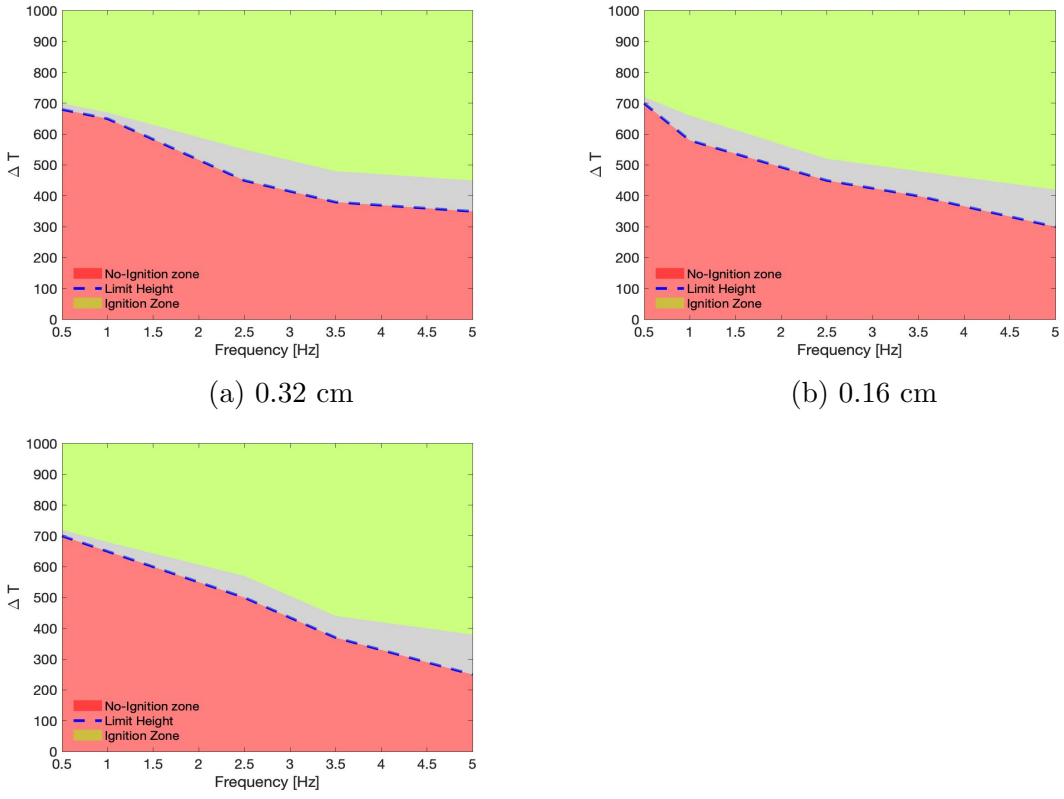


(a) 0.32 cm

(b) 0.16 cm

(c) 0.08 cm

Figure 5.5.1: Ignition and no ignition conditions observed in basswood sticks

Experiments and analysis have indicated the presence of a ignition and no-ignition

zone that is dependent on the temperature difference. The value of this difference is higher for lower flame frequencies as in the case for 0.5 Hz igniting at the 700 K point but ignition is seen at 5 Hz with a difference of 350 K for basswood of diameter 0.16 cm in figure 5.5.1b. The graph also indicates that the thickness of the fuel affects this term, $\Delta T$; a basswood stick of diameter 0.08 cm (figure 5.5.1c) the limit is at 250 K where as for diameter 0.32 cm (figure 5.5.1a) it's at 370 K. To standardize the different experiments, the temperature difference was fixed to approximately 700 K. This ensures that the fuel experiences the same difference in temperature but gives room to understand the effects of ignition in relation to flame frequencies.

# Chapter 6

# Heat Transfer Analysis

A simplified heat transfer model is presented here to describe heating and ignition of fine fuels in response to an intermittent flame. Numerous assumptions, including thermally-thin behavior, are taken in order to provide a first-order estimate of ignition time. The convective heat transfer correlations may not be entirely appropriate as it is not known whether the boundary layer fully forms within the short time pulsations impact the fuel, however without better forms available these correlations are used in this first analysis.

## 6.1 Lumped capacitance method

In a lumped capacitance model, the solid is assumed to have a spatially uniform temperature [47] with temperature only being a function of time, $T(t)$. While this assumption is not perfect for these fine fuels, it is a reasonable starting point for these calculations. Initial conditions are first assumed, i.e. that the fuel is at ambient

temperatures, for $T(0) = T_o$,

$$h(T_\infty - T)A_s = \rho c_p \frac{\partial T}{\partial t} V \tag{6.1}$$

The total energy transfer to a solid for the time from 0 to $t$ is then

$$Q = \rho c_p V(T_\infty - T_o) = m c_p \Delta T \quad \text{when} \quad t \to \infty \tag{6.2}$$

The time needed to heat a solid from $T_o$ to its current temperature $T$ is

$$t = \frac{\rho c_p}{h} \frac{V}{A_s} ln\left(\frac{T_\infty - T_o}{T_\infty - T}\right) \tag{6.3}$$

Rearranging equation 6.3 provides an equation for the temperature of a solid as a function of time,

$$T(t) = T_\infty + (T_o - T_\infty) e^{\frac{-h A_s t}{\rho c_p V}} \tag{6.4}$$

With radiation losses this equation becomes,

$$[h(T - T_\infty) + \epsilon\sigma(T^4 - T_\infty^4)]A_s = \rho V c_p \frac{dT}{dt} \tag{6.5}$$

To create a simplistic theoretical model in this research, equation 6.4 is used to determine the temperature of a fuel particle as a function of time.

### 6.1.1 Heat transfer characteristics

The Biot number, a ratio between conduction and convection thermal resistance [47] is computed as a function of time within the model to provide more information about the heat transfer characteristics of the input fuel,

$$Bi = \frac{hL_c}{k}. \tag{6.6}$$

The characteristic length used in the Biot number is calculated based on the volume $V$ of the fuel element and its area, $A_s$,

$$L_c = \frac{V}{A_s}. \tag{6.7}$$

The model is built with the capability of addressing both cylindrical and cuboidal geometries, as these were both used in experiments. For a cylinder, relevant equations to describe the geometry include the surface area,

$$A_s = \pi dH = 2\pi rH \tag{6.8}$$

Volume,

$$V = \frac{\pi d^2}{4}H = \pi r^2 H \tag{6.9}$$

Characteristic length,

$$L_c = \frac{d}{4} = \frac{r}{2} \tag{6.10}$$

and Biot number,

$$Bi = \frac{h}{k}\frac{r}{2}. \tag{6.11}$$

For a cuboid the equations are similar including the surface area,

$$A_s = 2HW \tag{6.12}$$

volume,

$$V = LHW \tag{6.13}$$

characteristic length,

$$L_c = \frac{L}{2} \tag{6.14}$$

and Biot number,

$$Bi = \frac{h}{k}\frac{L}{2}. \tag{6.15}$$

## 6.2 Convective heat transfer

To calculate convective heat transfer to individual fuel particles, including both heating and cooling, appropriate Nusselt number correlations must be determined. With the small diameter and velocities of the flame low Reynolds numbers can generally be assumed [47] For convective heating with $Pr > 0.6$ an appropriate

correlation for convective heating is

$$Nu_D = 1.15 Re_D^{1/2} Pr^{1/3}, \tag{6.16}$$

where $Nu_D$ is the Nusselt number, $Re_D$ is the Reynolds number based on the velocity measured from flame tracking and $Pr$ is the Prandtl number of air. Figure 6.2.1 shows a representative temperature rise of a 0.32 cm diameter basswood stick heated by 1000 K air.

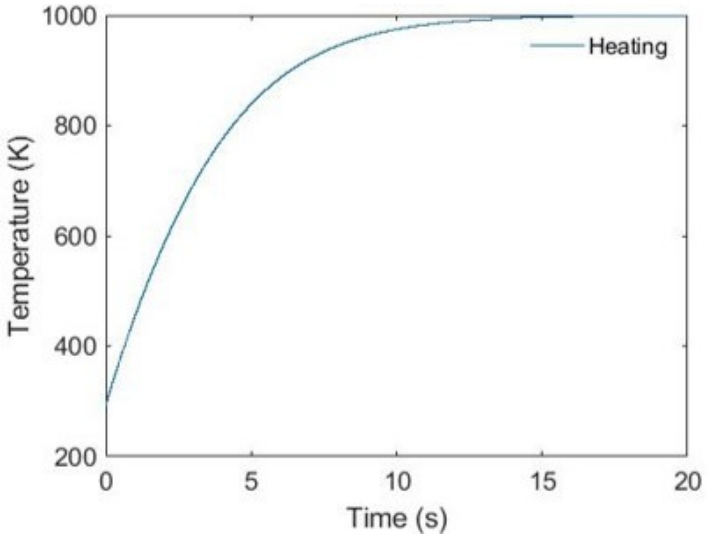


Figure 6.2.1: Constant convective heating result for a basswood stick of diameter 0.32 cm

For convective cooling, Churchill and Chu have recommended a single correlation for a wide Rayleigh number range of cylindrical elements [47],

$$Nu_D = \left[ 0.36 + \frac{0.387 Ra_D^{1/6}}{\left[ 1 + \left( \frac{0.559}{Pr} \right)^{9/16} \right]^{8/27}}, \right]^2 \tag{6.17}$$

where $[Ra_L < 10^{12}]$. Figure 6.2.1 shows the drop in stick temperature as a function of time for a basswood stick of diameter 0.32 cm convectively cooled from 1000 K.

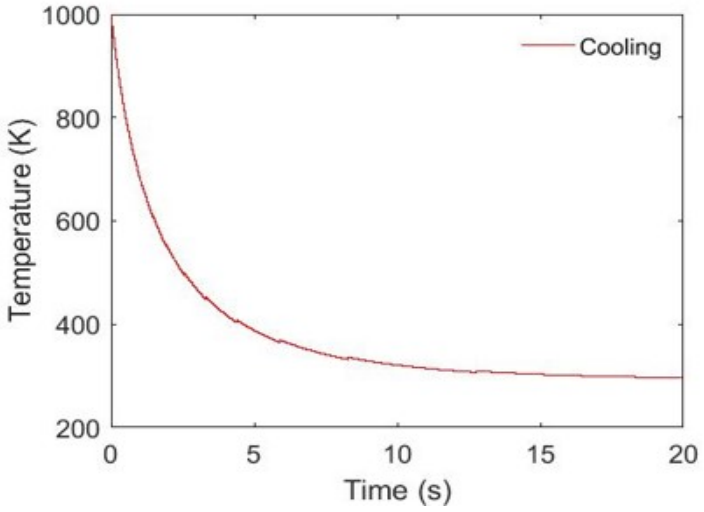


Figure 6.2.2: Constant cooling result for a basswood stick of diameter 0.32 cm

The foregoing correlations provide the average Nusselt number over the entire circumference of an iso-thermal cylinder. For a heated cylinder, local Nusselt numbers are influenced by boundary layer development. In our experiments short timescales may prohibit formation of a fully-developed boundary layer during some test duration, however the exact effect is unknown.

## 6.3 Simulation Results

The MATLAB code re-creates experiments by forming temperature profiles of gas surrounding fuels based on input audio files similar to the experiments and runs the heating portion of equation during the on duration and the cooling portion during the off duration for a user-specified testing period (60 seconds).

The theoretical model aims to re-create the experiments previously performed to estimate an ignition time for any type of fuel, with varying diameters, exposure to a wide range of flame frequencies and effectively simulating the intermittent heating condition using heat transfer equations. One of the vital standalone points in the model is its ability to create the audio files used in the form of a square/sine wave to run the simulation. This allows the user running the model to have flame frequencies anywhere from 0.1 Hz to 5 Hz. Figure 6.3.1 shows the result for the slowest ignition condition from the set of basswood experiments. In this simulation the model is using a 0.32 cm diameter basswood as fuel, exposed to a 0.5 Hz flame frequency which is the slowest ignition condition in the basswood tests.

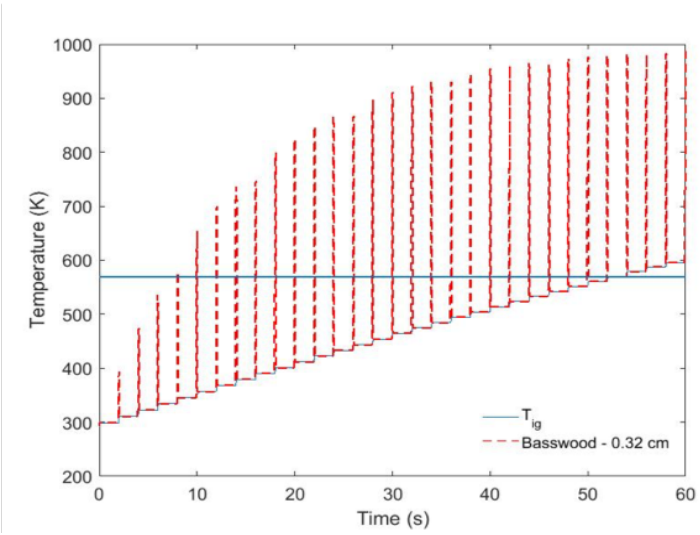


Figure 6.3.1: Simulation result for a basswood stick of diameter 0.32 cm exposed to a flame frequency of 0.5 Hz

The simulation indicates that ignition is achieved at approximately 50 seconds . The mean ignition time from tests is 36 seconds with a standard deviation of 14.4 seconds, therefore the simulation time comes just under the upper limit of the experimental

result, showing over-prediction. The input file being a square wave, has quick heating and cooling effects as the file logic is based on an on-off alternating approach.

Simulating the quickest scenario among the basswood tests shown in figure 6.3.2 results in an ignition time of 1.2 seconds which is just above the lower limits of a basswood test of 1.7 $\pm$ 0.35 seconds using a 0.08 cm stick exposed to a flame frequency of 5 Hz.

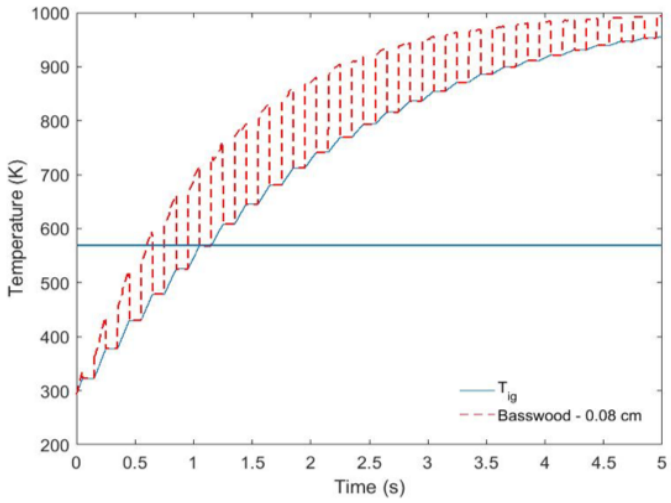


Figure 6.3.2: Simulation result for a basswood stick of diameter 0.08 cm exposed to a flame frequency of 5 Hz

Simulating all experimental conditions using this simulation has produced results that are often over-predicted or under-predicted. This is an indication that the equations and or assumptions made in the model have to be modified further to obtain more accurate results in the future. Trends, however, generally agree with experiments.

## 6.4 Comparison with experimental results

All experimental conditions using basswood sticks and the different flame frequencies used for center ignition tests were plotted and compared to the predicted results from the model. The compiled results are shown in figure 6.4.1.

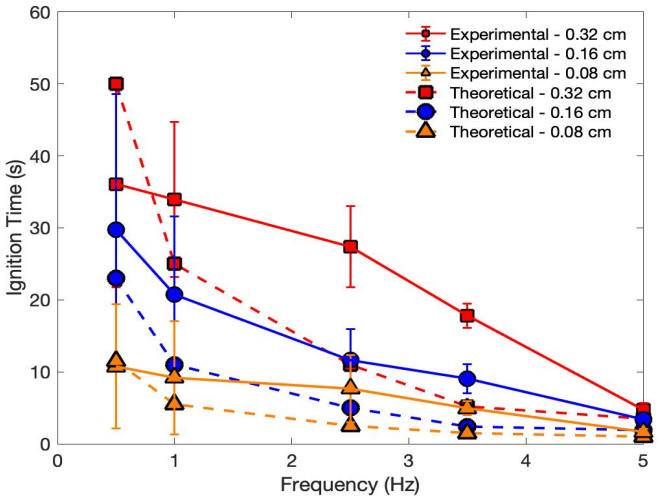


Figure 6.4.1: Plots with experimental and simulation results of ignition time for all basswood sticks

From the figure, it can be noted that there is a large variation in predicted and experimental ignition time when diameter of the fuel increases. The likely cause for this is due to the thermally thin assumption. It is possible that the thicker basswood sticks behave more like a thermally thick fuel at the higher diameters. In the thinnest fuel of basswood, 0.08 cm diameter, the experimental and predicted results match closely validating the thermally thin approach is true for extremely thin fuels. Table 6.1 shows the values for ignition time obtained both theoretically and experimentally. While the previously observed trend of ignition time decreasing with increase in flame

frequency, the same trend is seen from the simulation results.

Table 6.1: Basswood Experimental vs Predicted Ignition Time for Center Tests

| **Diameter** (cm) | **Frequency** (Hz) | **Mean Experimental Ignition time** (s) | **Predicted Ignition time** (s) |
|---|---|---|---|
| **0.32 cm** | 0.5 | 36.1 ± 14.4 | 50 |
| | 1 | 34 ± 10.75 | 25 |
| | 2.5 | 27.4 ± 5.6 | 11 |
| | 3.5 | 17.8 ± 1.7 | 5.2 |
| | 5 | 4.75 ± 0.89 | 3.5 |
| **0.16 cm** | 0.5 | 29.7 ± 18.9 | 23 |
| | 1 | 20.7 ± 10.9 | 11 |
| | 2.5 | 11.7 ± 4.3 | 5 |
| | 3.5 | 9.06 ± 2 | 2.4 |
| | 5 | 3.4 ± 0.5 | 1.9 |
| **0.08 cm** | 0.5 | 10.76 ± 8.65 | 11.5 |
| | 1 | 9.18 ± 7.89 | 5.5 |
| | 2.5 | 9.67 ± 4.66 | 2.5 |
| | 3.5 | 4.95 ± 0.95 | 1.5 |
| | 5 | 1.7 ± 0.35 | 1 |

The model can more accurately predict ignition times in the future by considering thermal gradients within the fuel. More work is required to be done before it can be used to predict results for all types of fuel or be embedded within a flame spread model.

# Chapter 7

# Conclusions and Future Work

## 7.1 Conclusion

Intermittent heating, as expected, is found to be capable of igniting fine fuels with intermittent flames over a wide range, although though this is slower than ignition times with constant flames. As the thickness of the fuel decreases, intermittent heating plays a reduced role, with the small mass of fuel rapidly heating. Somewhat larger fuels are more susceptible to the cooling period between pulses, significantly reducing ignition times.

In real wildland fires external radiation and convective cooling are also present during the flame spread process. Now that effects of intermittent heating have been quantified, a numerical scheme incorporating heating and cooling have been used to predict ignition times with all flame frequencies containing heating and cooling. The current theoretical model developed forms a simple and solid foundation to model the

effects of intermittent heating and cooling for fuels of different diameters and types. These pulsations seem to be a very important factor modeling wildland fire spread because fuels far from the fire front can be sporadically heated due to pulses from the flame, especially during high winds or steep slopes. An experimental platform now exists to validate future computations with each component of heating, useful for numerical predictions of ignition times and, hopefully, someday used in future wildfire simulations.

## 7.2 Future Work

Extensive work has been performed to uncover the trends and effects seen from intermittent heating in wildland fires. There is room to uncover more information about the intermittent flame region. Conducting experiments using steel or copper rods of different thickness to better understand heat transfer onto stick-shaped elements exposed to pulsating flames is a viable option. Using the data from these tests, the internal heating mechanisms can be modelled for both center and edge tests and heat transfer (Nusselt number) correlations formed for different fuel geometries. Inserting thermocouples onto the surface of fuels as well as within fuels can help uncover the thermal influences affecting the temperature of the fuels and verify their thermally thick or thin nature. Using live fuels would also help shed light on the effects of moisture content and different fuel properties on ignition time.

The model used here currently used has a lot of room for improvement. First, incorporating thermal gradients within the fuel appears important for thicker fuels.

In addition, using sine or triangular waves as the input audio file may help mimic the flame pulsations and allow MATLAB to solve the heat transfer correlations more proficiently. Evaluating the cooling equation with additional literature review sand computations could better the model and increase the time taken for fuels to cool to ambient temperature.

# Appendix A

# Additional Figures

## A.1 Dependence of distance from burner on ignition

Figure A.1.1 below shows the distance between the burner to the fuel sample that creates an ignition and no ignition region for each diameter of basswood. The grey zone depicts the area where ignition might or might not occur, depending on the environmental conditions.

For basswood,

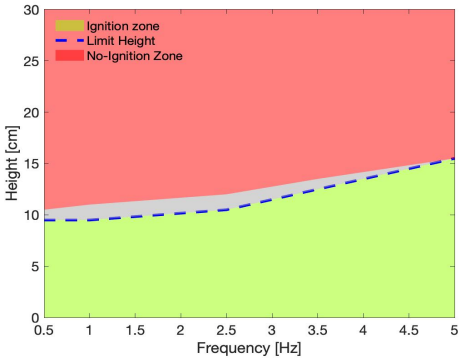


(a) 0.32 cm

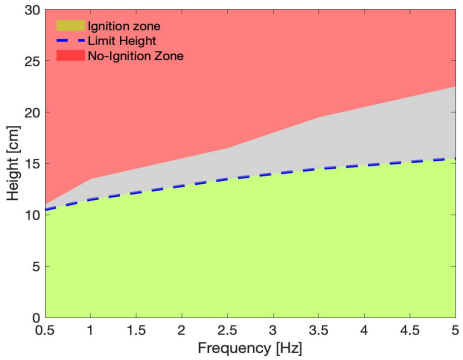


(b) 0.16 cm

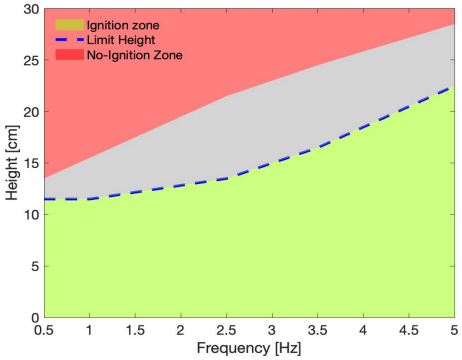


(c) 0.08 cm

Figure A.1.1: Distance from burner influencing ignition for basswood

Figure A.1.2 is a compiled image from Figure A.1.1 showing all basswood ignition data as a function of height on one graph.

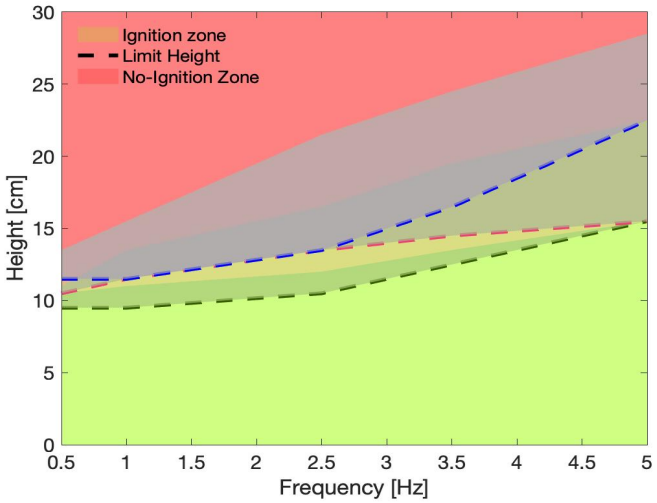


Figure A.1.2: Compiled basswood data as a function of distance from the burner influencing ignition

The same information is shown for birch wood in Figure A.1.3.

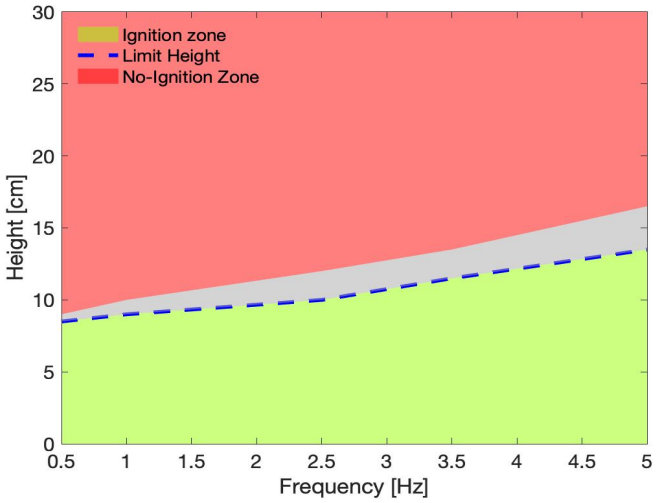


Figure A.1.3: Distance from burner influencing ignition of birch wood fuel

# References


[1] Jennifer R Marlon et al. "Climate and human influences on global biomass burning over the past two millennia". In: *Nature Geoscience* 1.10 (2008), p. 697.

[2] Meg A Krawchuk et al. "Global pyrogeography: the current and future distribution of wildfire". In: *PloS one* 4.4 (2009), e5102.

[3] Olga Pechony and Drew T Shindell. "Driving forces of global wildfires over the past millennium and the forthcoming century". In: *Proceedings of the National Academy of Sciences* 107.45 (2010), pp. 19167–19170.

[4] Mark A Finney et al. "On the need for a theory of wildland fire spread". In: *International journal of wildland fire* 22.1 (2013), pp. 25–36.

[5] Mark A Finney et al. "An examination of fire spread thresholds in discontinuous fuel bedsA". In: *International Journal of Wildland Fire* 19.2 (2010), pp. 163–170.

[6] Mark A Finney et al. "Role of buoyant flame dynamics in wildfire spread". In: *Proceedings of the National Academy of Sciences* 112.32 (2015), pp. 9833–9838.

[7] Stefan H Doerr and Cristina Santín. "Global trends in wildfire and its impacts: perceptions versus realities in a changing world". In: *Philosophical Transactions of the Royal Society B: Biological Sciences* 371.1696 (2016), p. 20150345.

[8] Anthony L Westerling et al. "Climate and wildfire in the western United States". In: *Bulletin of the American Meteorological Society* 84.5 (2003), pp. 595–604.

[9] *Is Global Warming Fueling Increased Wildfire Risks?* https://www.ucsusa.org.

[10] Jack D Cohen. "Reducing the wildland fire threat to homes: where and how much?" In: *In: Gonzales-Caban, Armando; Omi, Philip N., technical coordinators. Proceedings of the Symposium on Fire Economics, Planning, and Policy: Bottom Lines; 1999 April 5-9. San Diego, CA. Gen. Tech. Rep. PSW-GTR-173. Albany, CA: US Department of Agriculture, Forest Service, Pacific Southwest Research Station. p. 189-195.* 1999.

[11] Richard C Rothermel et al. *A mathematical model for predicting fire spread in wildland fuels.* Intermountain Forest & Range Experiment Station, Forest Service, US, 1972.

[12] Jack D Cohen. "Structure ignition assessment model (SIAM)". In: *In: Weise, David R.; Martin, Robert E., technical coordinators. The Biswell symposium: fire issues and solutions in urban interface and wildland ecosystems; February 15-17, 1994; Walnut Creek, California. Gen. Tech. Rep. PSW-GTR-158. Albany, CA: Pacific Southwest Research Station, Forest Service, US Department of Agriculture; p. 85-92.* Vol. 158. 1995.

[13] Breeanne K Jackson and S Mažeika P Sullivan. "Influence of wildfire severity on riparian plant community heterogeneity in an Idaho, USA wilderness". In: *Forest Ecology and Management* 259.1 (2009), pp. 24–32.

[14] Benjamin T Zinn. *Pulsating burner-controlling mechanisms and performance*. Tech. rep. Georgia Institute of Technology, 1987.

[15] O Delabroy et al. "A study of NOx reduction by acoustic excitation in a liquid fueled burner". In: *Combustion science and technology* 119.1-6 (1996), pp. 397–408.

[16] Patricia L Andrews. "Current status and future needs of the BehavePlus Fire Modeling System". In: *International Journal of Wildland Fire* 23.1 (2014), pp. 21–33.

[17] Mark A Finney. "FARSITE: Fire Area Simulator-model development and evaluation". In: *Res. Pap. RMRS-RP-4, Revised 2004. Ogden, UT: US Department of Agriculture, Forest Service, Rocky Mountain Research Station. 47 p.* 4 (1998).

[18] Frank A Albini and Elizabeth D Reinhardt. "Modeling ignition and burning rate of large woody natural fuels". In: *International Journal of Wildland Fire* 5.2 (1995), pp. 81–91.

[19] Aymeric Lamorlette. *Effect of harmonic heat flux variation on solid material piloted ignition*. Tech. rep. hal-00839634. HAL, 2013.

[20] J De Ris and L Orloff. "The role of buoyancy direction and radiation in turbulent diffusion flames on surfaces". In: *Symposium (International) on Combustion*. Vol. 15. Elsevier. 1975, pp. 175–182.

[21] Izabella Vermesi et al. "Pyrolysis and ignition of a polymer by transient irradiation". In: *Combustion and Flame* 163 (2016), pp. 31–41.

[22] Izabella Vermesi et al. "Pyrolysis and spontaneous ignition of wood under transient irradiation: Experiments and a-priori predictions". In: *Fire Safety Journal* 91 (2017), pp. 218–225.

[23] William H Frandsen. "Fire spread through porous fuels from the conservation of energy". In: *Combustion and Flame* 16.1 (1971), pp. 9–16.

[24] AG McArthur. "The Tasmanian bushfires of 7th February 1967, and associated fire behaviour characteristics". In: *Second Australian Conference on Fire. Australian Fire Protection Association, Melbourne*. 1968, pp. 25–48.

[25] John E Deeming. *National fire-danger rating system*. Vol. 84. Rocky Mountain Forest and Range Experiment Station, Forest Service, US Dept, 1972.

[26] Richard C Rothermel. *How to predict the spread and intensity of forest and range fires*. Tech. rep. USDA Forest Service, 1983.

[27] Hal E Anderson. *Heat transfer and fire spread*. Intermountain Forest and Range Experiment Station, Forest Service, US, 1969.

[28] RC Rothermel. “Some fire behavior modeling concepts for fire management systems”. In: *Proceedings of the 12th conference on fire and forest meteorology, Jekyll Island, Georgia.* SAF Publication, 1994, pp. 94–02.

[29] August Wilhelm Kuchler et al. “Vegetation mapping.” In: *Vegetation mapping.* (1967).

[30] Joe H Scott and Robert E Burgan. *Standard fire behavior fuel models: a comprehensive set for use with Rothermel's surface fire spread model.* Tech. rep. General Technical Report RMRS-GTR-153, 72 pp. USDA Forest Service, Rocky Mountain Research Station, 2005.

[31] Anne Ganteaume et al. “Spot fires: fuel bed flammability and capability of firebrands to ignite fuel beds”. In: *International Journal of Wildland Fire* 18.8 (2010), pp. 951–969.

[32] W Matt Jolly. “Sensitivity of a surface fire spread model and associated fire behaviour fuel models to changes in live fuel moisture”. In: *International Journal of Wildland Fire* 16.4 (2007), pp. 503–509.

[33] Wallace L Fons. “Analysis of fire spread in light forest fuels”. In: *Journal of Agricultural Research* 72.3 (1946), pp. 93–121.

[34] Jozef Hladkỳ and Roman Ďurikovič. “Fire Simulation in 3D Computer Animation with Turbulence Dynamics including Fire Separation and Profile Modeling”. In: *International Journal of Networking and Computing* 8.2 (2018), pp. 186–204.

[35] Jack D Cohen and Mark A Finney. "An examination of fuel particle heating during fire spread". In: *VI International Conference on Forest Fire Research*. 2010, pp. 15–17.

[36] GM Byram et al. *An experimental study of model fires*. Tech. rep. SOUTHERN FOREST FIRE LAB MACON GA, 1964.

[37] Richard C Rothermel and Hal E Anderson. *Fire spread characteristics determined in the laboratory*. Inter-mountain Forest & Range Experiment Station, Forest Service, US, 1966.

[38] FA Albini. "A physical model for firespread in brush". In: *Symposium (International) on Combustion*. Vol. 11. Elsevier. 1967, pp. 553–560.

[39] M Vogel and FA Williams. "Flame propagation along matchstick arrays". In: *Combustion Science and Technology* 1.6 (1970), pp. 429–436.

[40] George F Carrier, Francis E Fendell, and Michael F Wolff. "Wind-aided firespread across arrays of discrete fuel elements. I. Theory". In: *Combustion Science and Technology* 75.1-3 (1991), pp. 31–51.

[41] Terry L Clark et al. "Analysis of small-scale convective dynamics in a crown fire using infrared video camera imagery". In: *Journal of Applied Meteorology* 38.10 (1999), pp. 1401–1420.

[42] Janice Coen, Shankar Mahalingam, and John Daily. "Infrared imagery of crown-fire dynamics during FROSTFIRE". In: *Journal of Applied Meteorology* 43.9 (2004), pp. 1241–1259.

[43] Jean-Francois Sacadura. "Radiative heat transfer in fire safety science". In: *ICHMT DIGITAL LIBRARY ONLINE*. Begel House Inc. 2004.

[44] S Sen and IK Puri. "Thermal radiation modeling in flames and fires". In: *Transport Phenonema in Fires* (2008), p. 301.

[45] Peter G Baines. "Physical mechanisms for the propagation of surface fires". In: *Mathematical and Computer Modelling* 13.12 (1990), pp. 83–94.

[46] NJ De Mestre et al. "Uniform propagation of a planar fire front without wind". In: *Combustion Science and Technology* 65.4-6 (1989), pp. 231–244.

[47] Frank P Incropera et al. *Fundamentals of heat and mass transfer*. Wiley, 2007.

[48] RO Weber. "Wildland fire spread models". In: *Forest Fires*. Elsevier, 2001, pp. 151–169.

[49] DR Packham and A Pompe. "Radiation temperatures of forest fires". In: *Australian Forest Research* 5.3 (1971), pp. 1–8.

[50] David Frankman et al. "Measurements of convective and radiative heating in wildland fires". In: *International Journal of Wildland Fire* 22.2 (2013), pp. 157–167.

[51] Roger D Ottmar et al. "An overview of the fuel characteristic classification systemfffdfffdfffdquantifying, classifying, and creating fuelbeds for resource planning". In: *Canadian Journal of Forest Research* 37.12 (2007), pp. 2383–2393.

[52] Andrew L Sullivan. "Wildland surface fire spread modelling, 1990–2007. 1: Physical and quasi-physical models". In: *International Journal of Wildland Fire* 18.4 (2009), pp. 349–368.

[53] Andrew L Sullivan. "Wildland surface fire spread modelling, 1990–2007. 2: Empirical and quasi-empirical models". In: *International Journal of Wildland Fire* 18.4 (2009), pp. 369–386.

[54] Andrew L Sullivan. "Wildland surface fire spread modelling, 1990–2007. 3: Simulation and mathematical analogue models". In: *International Journal of Wildland Fire* 18.4 (2009), pp. 387–403.

[55] Michael Gollner et al. *Towards data-driven operational wildfire spread modeling: A report of the nsf-funded wifire workshop*. Tech. rep. University of Maryland, 2015.

[56] August Kundt. "Ueber eine neue Art akustischer Staubfiguren und über die Anwendung derselben zur Bestimmung der Schallgeschwindigkeit in festen Körpern und Gasen". In: *Annalen der Physik* 203.4 (1866), pp. 497–523.

[57] U Behn. "U. Behn und F. Kiebitz, Ann. d. Phys., 4 S., 12, p. 421, 1903". In: *Ann. d. Phys.* 12 (1903), p. 421.

[58] George W Ficken and Francis C Stephenson. "Rubens flame-tube demonstration". In: *The Physics Teacher* 17.5 (1979), pp. 306–310.

[59] Duan Jihui and Charles TP Wang. "Demonstration of longitudinal standing waves in a pipe revisited". In: *American Journal of Physics* 53.11 (1985), pp. 1110–1112.

[60] George F Spagna Jr. "Rubens flame tube demonstration: A closer look at the flames". In: *American Journal of Physics* 51.9 (1983), pp. 848–850.

[61] Harold A Daw. "A two-dimensional flame table". In: *American Journal of Physics* 55.8 (1987), pp. 733–737.

[62] Harold A Daw. "The normal mode structure on the two-dimensional flame table". In: *American Journal of Physics* 56.10 (1988), pp. 913–915.

[63] Michael D Gardner, Kent L Gee, and Gordon Dix. "An investigation of Rubens flame tube resonances". In: *The Journal of the Acoustical Society of America* 125.3 (2009), pp. 1285–1292.

[64] *Nikon D7000*. https://www.nikonusa.com.

[65] *GoPro Hero 6*. https://gopro.com/update/hero6.

[66] Ajay V Singh and Michael J Gollner. "A methodology for estimation of local heat fluxes in steady laminar boundary layer diffusion flames". In: *Combustion and Flame* 162.5 (2015), pp. 2214–2230.

[67] *Emissivity Table*. https://www.thermoworks.com/$emissivity_table$.

[68] Allan J Zuckerwar. "Speed of sound in real gases. I. Theory". PhD thesis. ASA, 1996.

[69] DS Chamberlin and A Rose. "The flicker of luminous flames". In: *Proceedings of the Symposium on Combustion*. Vol. 1. Elsevier. 1948, pp. 27–32.

[70] *Engineering ToolBox*. https://www.engineeringtoolbox.com/.

[71] James Quintiere. *Fundamentals of fire phenomena*. Wiley, 2006.